Cenozoic Tectonics, Magmatism, and Stratigraphy of the Snake River Plain–Yellowstone Region and Adjacent Areas themed issue

Geochemical and paleomagnetic variations in basalts from the Wendell Regional Aquifer Systems Analysis (RASA) drill core: Evidence for magma recharge and assimilation–fractional crystallization from the central Snake River Plain, Idaho

Marlon M. Jean[1,*], John W. Shervais[2], Duane E. Champion[3], and Scott K. Vetter[4]
[1]*Department of Geology, Northern Illinois University, Davis Hall 312, DeKalb, Illinois 60115, USA*
[2]*Department of Geology, Utah State University, 4505 Old Main Hill, Logan, Utah 84322–4505, USA*
[3]*U.S. Geological Survey, 345 Middlefield Road, Menlo Park, California 94025, USA*
[4]*Department of Geology, Centenary College, Shreveport, Louisiana 71134, USA*

ABSTRACT

The temporal and magmatic evolution of central Snake River Plain (SRP; Idaho, USA) olivine tholeiites erupted within the past 4 m.y. is evaluated here. This investigation correlates and merges both geochemical and paleomagnetic measurements to constrain the volcanic history recovered from the 340 m Regional Aquifer Systems Analysis (RASA) test well located near Wendell, Idaho. Only a handful of studies have accomplished this task of shedding light on the chemical stratigraphy of the SRP and the petrogenesis of basalts with depth, and therefore through time.

Paleomagnetic relationships suggest that time breaks between individual lava flows represent a few years to decades, time breaks between flow groups represent at least a couple of hundred years or possibly much longer, while significant hiatuses in volcanism, revealed by thick sediment packages or polarity reversals (both are evidenced in this well), are inferred to last thousands to tens of thousands of years. Major element geochemistry from 52 basaltic lava flows demonstrates near primitive compositions (i.e., ~10 wt% MgO) and tholeiitic iron enrichment trends, similar to lavas from the eastern SRP. Trace element concentrations are similar to those of ocean island basalts, with enriched Ba and Pb, and light rare earth element (REE)/heavy REE ratios similar to those of many Neogene volcanics of the western Cordillera. When combined, we identify a total of 11 flow groups, which we also classify as fractionation or recharge on the basis of decreasing or increasing MgO weight percent with depth.

Taking into consideration these trends, we review the potential recharge, fractionation, and assimilation processes that characterize much of SRP olivine tholeiite, and conclude that assimilation, in combination with fractional crystallization, is the dominant petrogenesis for the basalts in the central SRP. Although fractionation of Wendell parent magmas was accompanied by assimilation of crustal material, this could not have been assimilation of ancient cratonic crust. The geochemical cycles observed in this well are inferred to represent fractionation and recharge of basaltic magma from a series of sill-like layered mafic intrusions located in the middle crust, similar to what has been proposed for the processes that control the eruptive history of basalts in the eastern SRP.

INTRODUCTION

The Yellowstone–Snake River Plain (YSRP; western USA) is a broad, flat, arcuate physiographic province that covers much of southern Idaho, culminating in the Yellowstone Plateau. Volcanic activity associated with this province links the voluminous ca. 17 Ma flood basalts of the Miocene Columbia River province in southeastern Oregon to Quaternary volcanic centers at Island Park, Idaho, and Yellowstone National Park in Wyoming (e.g., Smith and Braile, 1993, 1994; Pierce et al., 2002). Plains-type basalt (Greeley, 1982) erupted from numerous shield volcanoes that now form an axial topographic volcanic high down the middle of the eastern Snake River Plain (SRP). Petrologic studies have shown that this basalt is mostly olivine tholeiite (e.g., Geist et al., 2002a, 2002b; Hughes et al., 2002; Shervais et al., 2005), with relatively large ranges in major and trace element composition that require some combination of fractional crystallization, crustal assimilation, and periodic recharge of magma chambers via batch melts from the upper mantle (Miller and Hughes, 2009).

Several deep drill holes are located along the SRP (Fig. 1A). However, for the past 25 years most of this drilling has been carried out in the eastern SRP at Idaho National Laboratory (INL). This site is northwest of the axial volcanic high that separates a depression along the southeastern margin of the plain (the Snake River drainage) from a similar depression along its northwestern margin (internal drainage of the Big Lost River, Little Lost River, and Birch Creek). Investigations into INL drill cores have been directed toward understanding the local volcanic stratigraphy and subsurface geology, groundwater flow, regional geochemistry, age relations via paleomagnetism, and petrogenetic processes responsible for creating the volcanic rocks of the SRP (e.g., Champion et al., 2002, 2011; Geist et al., 2002a, 2002b; Hughes et al., 2002; Link and Mink, 2002; Shervais et al., 2006a; Hanan et al., 2008; Miller and Hughes, 2009). However, only a few of these studies have focused on the chemical stratigraphy of SRP basalts and their petrogenesis with depth, and therefore through time; these studies also recorded upsection increase or decrease in

*Corresponding author. Present address: Institut fur Mineralogie, Leibniz Universitaet Hannover, Callinstr. 3, 30167 Hannover, Germany; mmj@niu.edu.

Geosphere; October 2013; v. 9; no. 5; p. 1319–1335; doi:10.1130/GES00914.1; 6 figures; 3 tables; 1 supplemental file.
Received 19 February 2013 ♦ Revision received 20 June 2013 ♦ Accepted 14 August 2013 ♦ Published online 13 September 2013

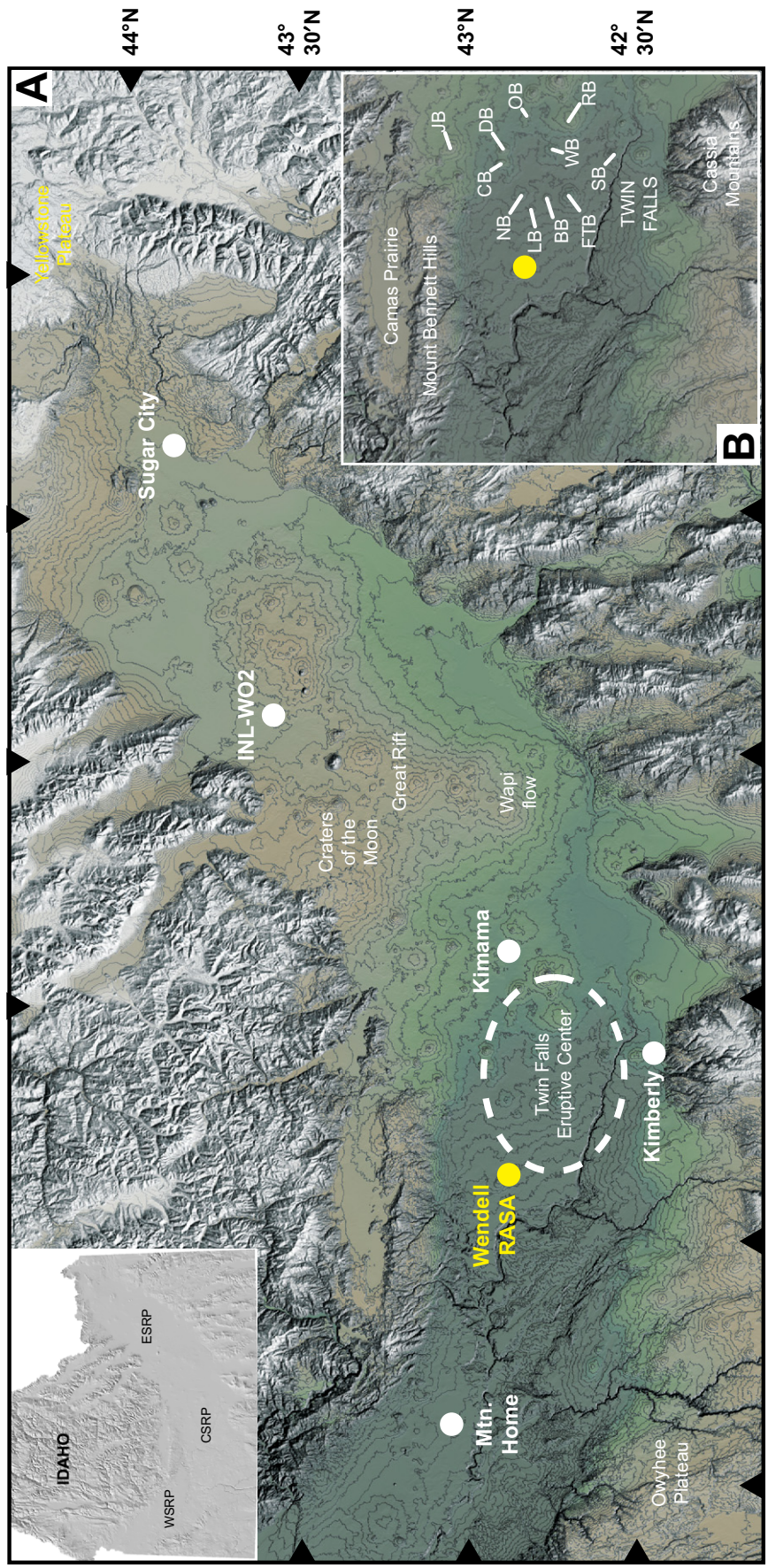

Figure 1. Snake River Plain (SRP; E—eastern; W—western; C—central) location map. (A) Approximate location of the Wendell Regional Aquifer Systems Analysis (RASA) drill hole (yellow circle) along with other Yellowstone–Snake River Plain drill holes (white circles), e.g., Sugar City (0.7 km), Idaho National Laboratory (INL–WO2; 1.52 km), Project Hotspot–Kimama (1.91 km), Project Hotspot–Kimberly (1.96 km), and Mountain Home (1.3 km). (B) Inset of the regional features of the central SRP (CSRP), includes the Camas Prairie, Cassia Mountains, Mount Bennett Hills, and the Twin Falls eruptive center. The location of the Wendell drill hole is shown in relation to nearby volcanic vents: Bacon Butte (BB), Crater Butte (CB), Dietrich Butte (DB), Flat Top Butte (FTB), Johnson Butte (JB), Lincoln Butte (LB), Notch Butte (NB), Owinza Butte (OB), Rocky Butte (RB), Skeleton Butte (SB), and Wilson Butte (WB).

major elements and incompatible elements and attributed these trends to complex processes of fractionation and mixing during magma evolution, but did not pair these trends to any time constraints.

Unlike the extensive drilling in the eastern SRP, the volcanic stratigraphy and geochemistry of subsurface lava flows from the central SRP have only been reported by us (this study) and from Kimama (basalt and sediments) and Kimberly (basalt, sediments, and rhyolite) drill cores from Project Hotspot (Potter et al., 2011; Shervais et al., 2011, 2012). The Wendell Regional Aquifer Systems Analysis (RASA) hydrologic test well is a 342.3 m test hole drilled near Wendell, Idaho, and was part of the SRP regional aquifer study (Whitehead and Lindholm, 1985). The main purpose for this drilling was to determine the subsurface geology and its controls on water movement in the ~60 km reach of the Snake River from Twin Falls to Bliss, and in particular in the vicinity of Thousand Springs, the major discharge area for the Snake River Aquifer of the eastern SRP. The hole penetrated an upper basalt unit from 0.3 to 122.8 m, an intermediate unconsolidated sedimentary unit from 122.8 to 179.8 m, a lower basalt unit from 179.8 to 327 m, and another sedimentary sequence from 327 m to total depth. This stratigraphy approximates the stratigraphy found in the upper part of the Kimama drill core, drilled ~30 km to the east. A lithologic log of the Kimama core shows that it consists almost entirely of basalt, with thin intercalations of loess-like sediment in the upper 200 m of the hole, and somewhat thicker beds of fluvial gravels, sands, and silts in the lower 300 m of the hole (Shervais et al., 2012). The Kimama drill core, however, is more than 5 times greater in depth than the section sampled at Wendell.

To assess the construction of basaltic lavas in the central SRP and their evolution, we present a detailed petrologic, paleomagnetic, and geochemical investigation from the Wendell core. Our main purpose is to establish the nature and extent of chemical changes though time at a single location, where the physical and chemical aspects of the crust and mantle lithosphere are relatively fixed. Using paleomagnetic measurements, we first correlate individual lava flows and flow groups with paleomagnetic time scales. The identification of these magnetic groups and the hiatuses between them is entirely independent of chemistry; however, by merging geochemical and paleomagnetic measurements, we define flow groups that are both chemically related and erupted within relatively short time spans. We use geochemical data to demonstrate the chemical stratigraphy and designate flow groups that represent periods of magma fractionation or recharge. We also use geochemical data to demonstrate that the lavas in the Wendell core formed through assimilation–fractional crystallization, with the assimilating material being that of previously intruded mafic rocks, likely sourced from differentiated mafic sills within the crust. This study allows us to expand our knowledge of the fractionation and magma recharge history of basalts farther west of the INL site and address current models of basaltic volcanism in the YSRP and how these relate to the crustal processes at work in the central SRP.

REGIONAL SETTING

The central SRP contains basalt, rhyolite, and lacustrine sediment (Armstrong et al., 1975; Pierce and Morgan, 1992). It is considered a transitional province that lies between the northwest-trending, normal fault–bounded western plain and the predominantly downwarped, not-fault-bounded eastern plain. It is defined loosely as that part of the eastern SRP between the Owyhee Plateau, a highland in southwestern Idaho underlain by mainly Miocene rhyolites, and the Great Rift, a north-northwest–trending fissure that extends for ~50 km from Craters of the Moon National Monument on the north to the Wapi lava field on the south (Kuntz et al., 1982, 1992).

The main regional geologic features of the central SRP include the Twin Falls eruptive center and the Mesozoic, Paleozoic, and Miocene rocks of the highlands located to the south and north of Twin Falls, Idaho (e.g., Kauffman et al., 2011; Fig. 1). The Twin Falls eruptive center is a buried rhyolite eruptive center, observable today by an ovoid-shaped gravity anomaly (Shervais et al., 2011). Major ignimbrite volcanism principally occurred in the Twin Falls eruptive center from 8 to 10 Ma (Perkins et al., 1995). Rhyolitic volcanism ended in the Twin Falls eruptive center ca. 6 Ma (Armstrong et al., 1975; Bonnichsen and Godchaux, 2002, and references therein). The southern highlands, including the Cassia Mountains (South Hills), are underlain mainly by Miocene silicic volcanic rocks, which generally flowed southward to cover earlier Tertiary volcanic rocks and Mesozoic and Paleozoic marine sedimentary rocks. The Cassia Mountains and other parts of the southern highlands mark the separation between the Basin and Range Province and the YSRP province (Bonnichsen and Godchaux, 2002). The northern highlands, including the Mount Bennett Hills, are underlain by Miocene silicic volcanic rocks similar to those in the southern highlands and, in turn, overlie older Tertiary volcanic rocks of the Challis Formation and granitic rocks of the Idaho Batholith. The Mount Bennett Hills are bordered to the north by the Camas Prairie, a Pliocene–Pleistocene east-west–oriented half-graben, in which there are abundant accumulations of late Pliocene and Pleistocene YSRP-type basalt and fluvial and lacustrine sediment (Bonnichsen and Godchaux, 2002).

The area surrounding Wendell includes late Neogene to Quaternary basalts, erupted from shield volcanoes clustered along the axis of the plain (Fig. 1B). These shield volcanoes overlie rhyolite from the Twin Falls eruptive center (Bonnichsen and Godchaux, 2002; Shervais et al., 2005). Rhyolite, however, was not intersected in this drill core. This area was mapped in detail (Kauffman et al., 2005; Cooke et al., 2006a, 2006b; Matthews et al., 2006a, 2006b; Shervais et al., 2006b, 2006c) and summarized on the Twin Falls 30′ × 60′ quadrangle geologic map (Kauffman et al., 2011). Older shield volcanoes (older than 1.0 Ma, e.g., Flat Top Butte, Johnson Butte) have subdued topography, radial drainages, and well-developed loess covers and soils. Many of the older vents appear smaller than the younger vents because their flanks have been partially buried by younger lava flows (e.g., Skeleton Butte, Bacon Butte, and Lincoln Butte). Flow surfaces from younger vents (younger than 1.0 Ma, e.g., Owinza Butte, Rocky Butte, Notch Butte, and Wilson Butte) are characterized by rugged chaotic topography, with inflated flow fronts, collapsed flow interiors, ridges, and collapse pits. The surfaces of flows from vents of intermediate age (e.g., Crater Butte and Dietrich Butte) have nearly continuous loess mantles of variable thickness and well-developed soils, but lack well-defined surface drainages (Shervais et al., 2005). Lava flows emanating from some of the buttes mentioned here were intersected in the Wendell RASA well, e.g., lava flows from Notch Butte were intersected near the top of the Snake River Group section.

CORE OBSERVATIONS

Stratigraphy

Volcanic rocks intersected in the Wendell well include two basalt sections, each >100 m thick, and two ash deposits. The upper basalt section, identified as Snake River Group, is typical of Quaternary tholeiitic basalt of the eastern SRP and constitutes the first 123 m of core (Fig. 2A). A lower basalt section, identified as Tertiary Idaho Group, was intersected from 179.8 to 327.1 m; the term Banbury basalt is often used for lack of a formal name for these older basalts. Whitehead and Lindholm (1985) identified 25 lava flows in the Snake River Group section and 27 lava flows in the Idaho Group

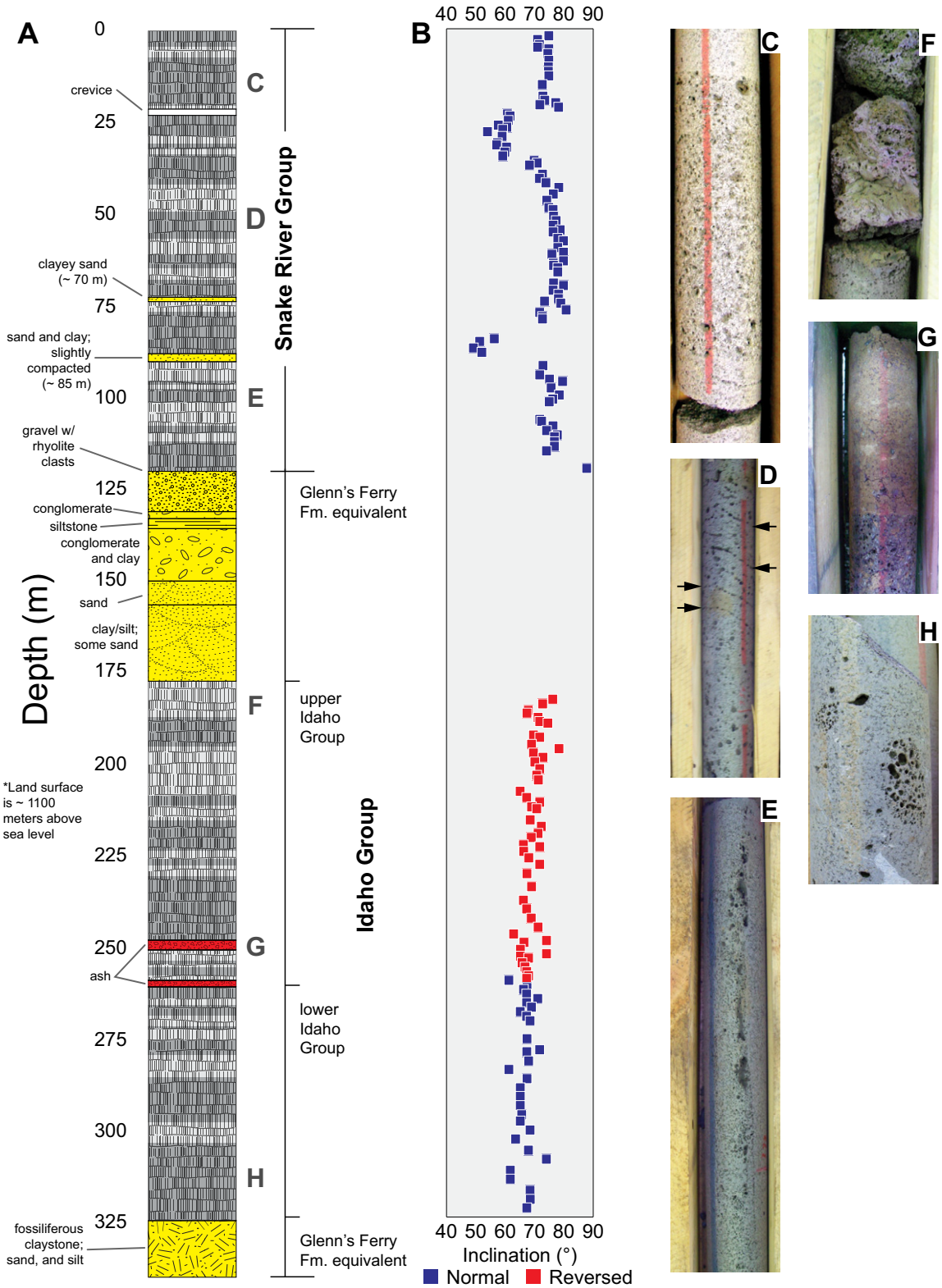

Figure 2. (A) Lithologic log of Wendell Regional Aquifer Systems Analysis (RASA) test hole 7S–15E–12CBA5 (originally 7S–15E–12CBA1; modified from Whitehead and Lindholm, 1985). Alternating shades of gray denote individual lava flows. Locations of C–H are shown next to lithologic log. (B) Paleomagnetic inclinations. (C–E) Volcanic features observed within the Snake River Group section. (C) Flow breakouts (more plagioclase-rich section). (D) Vesicle sheets or segregation zones (black arrows point to sheets). (E) Vesicle pipes. (F–H) Volcanic features observed within the Idaho Group section. (F) Ropey and/or agglutinate features. (G) Ash layer at 250 m. (H) Autoliths and/or remobilized spatter.

section, ranging from ~1 to 13 m thick (Fig. 2A). Contacts between lava flows were identified using the occurrence of brecciated flow tops and sediment intervals, the location of grayish-red purple basalt with bigger vesicles overlying less vesicular medium gray basalt, or through petrography. Two reddish-orange ash deposits are observed near the middle of the Idaho Group, at ~250 and ~260 m below surface (mbs; Fig. 2A). The lower ash unit separates the upper Idaho member (180–260 mbs) from the lower Idaho member (260–327 mbs) and also occurs at a paleomagnetic reversal (Fig. 2B).

Four sedimentary sections were also observed in the Wendell well. Two thin sediment horizons, <3 m thick, are observed in the Snake River Group at ~70 m (clayey sand) and 85 m (slightly compacted sand and clay). The largest sediment interval is 57 m thick, observed from 122.8 to 179.8 m, and separates Snake River Group basalt from Idaho Group basalt (Fig. 2A). This package fines downward, and includes gravels and conglomerates with clasts of rhyolite at the top to sand, clay, and silt horizons at the bottom (Whitehead and Lindholm, 1985). Another significant sediment package, composed of claystone and sand and silt, underlies lower Idaho Group basalt, and makes up the bottom 15 m of the hole. These sediments have been found to contain conispiral gastropods and plant fragments (Whitehead and Lindholm, 1985).

Lithology

Basalt from the Snake River Group is vesicular and distinctively grayish-red purple. The central part is generally much less vesicular and is mostly gray. The lower part is more crystalline, gray, and has a more sugary or equigranular texture. Basalt from the Snake River Group is typically more vesicular than Idaho Group basalt. Some pervasive features from these lavas include plagioclase-rich and olivine-poor horizons (Fig. 2C), amygdules filled with secondary minerals, e.g., calcite, pyrite, or zeolites, vesicle sheets or segregation zones (~51.8 mbs; Fig. 2D), and vesicle pipes (~100.5 mbs; Fig. 2E).

The top 30 m of the upper Idaho Group basalt is a very cindery, scoriaceous zone with agglutinate and ropey features (Fig. 2F). Below this zone, basalt is crystalline with few fractures and vesicles. Throughout much of this part of the core, basalt has a sugary or equigranular texture with varying degrees of alteration, i.e., secondary mineralization of calcite and alteration to clay. Whitehead and Lindholm (1985) also recognized fluorite and what they characterized as serpentinized material in their description of this core. The ash layers overlie strongly oxidized basalt (Fig. 2G). Scoriaceous basalt clasts were identified within the matrix of the 250 mbs ash. Massive lava flows that underlie the lower ash unit most likely represent a ponded flow or lava lake; autoliths, interpreted as remobilized spatter, are observed throughout this section (Fig. 2H).

METHODS

Paleomagnetic

Paleomagnetic inclination and polarity measurements were conducted on hundreds of subsamples using the Idaho National Laboratory Lithologic Core Storage Library protocols described in Davis et al. (1997). These samples were collected independently of samples collected for chemical analysis. Attempts were made to take at least seven paleomagnetic samples from the lava flows originally identified by Whitehead and Lindholm (1985), using a drill press with a 2.5-cm-diameter diamond core bit, and drilling at right angles to the vertical axis of the original core. The core plugs were trimmed to 2.2 cm lengths, and the inclination, unoriented declination, and intensity of magnetizations were measured using a cryogenic magnetometer. Progressive alternating-field (AF) demagnetization using a commercial tumbling demagnetizer was performed on one sample from each core plug to remove any components of secondary magnetization. Mean inclination values for each lava flow and 95% confidence limits about the mean value were calculated using the method of McFadden and Reid (1982). These inclination and polarity data obtained from successive lava flows in stratigraphic order allow us to assess whether these flows have similar or different remanent magnetizations.

Analytical

All 62 basalt samples from the 52 lava flows, in addition to one of the ash layers, were analyzed for whole-rock major and trace elements. Samples for major element analysis were first crushed in a GyralGrinder Shatterbox inside a tungsten carbide vessel and ground again with an agate mortar and pestle. Following grinding, sample powders were calcined at 800 °C for 24 h then mixed with 6 g of a Claisse flux, with a composition of 35% Li-tetraborate and 65% Li-metaborate; 6 drops of LiI was added as a releasing agent. That combination was heated using a Claisse fluxer to convert the mixtures to glass beads and analyzed on the MagiX Pro X-ray fluorescence (XRF) instrument at California State University (Fresno). Rare earth and other trace element concentrations were measured using the PerkinElmer 6000 inductively coupled plasma–mass spectrometer (ICP-MS) at Centenary College (Shreveport, Louisiana); ~60 mg of each sample was first dissolved in 2 mL HF and 3 mL HNO_3 for 3 h: watch glasses prevented evaporation. After target time was reached, watch glasses were removed and samples taken to dryness. Following this step, another 3 mL HNO_3 was added and samples were left at 50 °C overnight, then dried down at 90 °C. After this second drying, another 3 mL HNO_3 was added and dried down immediately. The sample was brought into solution with 2–3 mL of 50% HNO_3 and brought up to 50 mL total by adding 5% HNO_3. This analytical protocol was modified from Jenner et al. (1990) and Neal (2001).

Table 1 demonstrates the reproducibility of U.S. Geological Survey (USGS) standard W-2 (USGS Geochemical Reference Materials; http://crustal.usgs.gov/geochemical_reference_standards/index.html), via XRF at California State University (Fresno) (for major elements) and ICP-MS at Centenary College (for trace elements). This study was able to reproduce this standard within standard deviation of the preferred values. This is reflected in the low relative standard errors, generally <3.0%. The instruments at both labs also recorded similar or lower standard deviations for the W-2 standard.

RESULTS

Paleomagnetic

This study identified stratigraphic intervals that displayed a normal or reverse polarity, as well as intervals with similar or different inclination values. There are two normal polarity sequences and one reverse polarity sequence. In addition, there are seven inclination intervals in the Wendell RASA well: five within the Snake River Group and two within the Idaho Group.

Within the Snake River Group, there are three intervals with steep inclinations, separated by two intervals with shallow inclinations. The first shallow inclination interval (24.3–35.3 mbs) is composed of 13 paleomagnetic samples, with an inclination range of 54°–62°, mean of 59°. The second shallow inclination interval (85.3–88.4 mbs) is composed of 4 paleomagnetic samples and overlies a sediment interbed; inclination ranges from 49° to 56°, with a mean inclination of 52° (Fig. 2B). Paleomagnetic samples taken from the upper Idaho Group have reversed magnetic polarity, with nearly constant reversed inclination, i.e., –68° to –71°. The lower Idaho Group has normal polarity with an inclination that ranges from 65.9° to 68.1° (Fig. 2B).

TABLE 1. REPRODUCIBILITY OF U.S. GEOLOGICAL SURVEY STANDARD W-2

	W-2 preferred values	W-2 measured values	Standard deviation	Relative standard error (%)
SiO_2	52.68 ± 0.29*	52.84	0.21	0.2
TiO_2	1.06 ± 0.01	1.09	0.01	1.9
Al_2O_3	15.45 ± 0.16	15.19	0.11	1.2
Fe_2O_3	10.83 ± 0.21	10.79	0.18	0.3
MnO	0.167 ± 0.004	0.17	–	1.3
MgO	6.37 ± 0.058	6.38	0.09	0.1
CaO	10.86 ± 0.078	11.22	0.09	2.3
Na_2O	2.2 ± 0.037	2.19	0.02	0.3
K_2O	0.626 ± 0.012	0.6	0.008	3.0
P_2O_5	0.13 ± 0.03	0.112	0.002	4.5
Sc	35.9 ± 0.8†	34.3	1.3	3.2
V	268 ± 10.0	271	13.4	0.8
Rb	21 ± 1.0	22	0.2	3.3
Sr	196 ± 5.0	222	3.5	8.8
Y	22 ± 1.0	17.2	0.6	
Zr	92 ± 4.0	90	5.1	1.6
Nb	7.5 ± 0.6	7.0	0.3	4.9
Ba	170 ± 11*	167	4.7	1.3
La	10.8 ± 0.5	10.7	0.5	0.7
Ce	23.4 ± 0.7	22.7	1.3	2.2
Pr	3.0 ± 0.1	2.9	0.1	2.4
Nd	13 ± 0.5	13	0.1	0.0
Sm	3.3 ± 0.08	3.3	0.10	0.0
Eu	1.08 ± 0.03	1.1	0.02	1.3
Gd	3.66 ± 0.12	3.7	0.10	0.8
Tb	0.62 ± 0.03	0.6	0.02	2.3
Dy	3.79 ± 0.09	3.9	0.20	2.0
Ho	0.79 ± 0.03	0.8	0.02	0.9
Er	2.5 ± 0.1*	2.6	0.1	2.8
Tm	0.38 ± 0.02*	0.35	0.01	5.8
Yb	2.1 ± 0.2*	2.2	0.1	3.3
Lu	0.31 ± 0.01	0.3	0.02	2.3
Hf	2.6 ± 0.18*	2.7	0.10	2.7
Ta	0.47 ± 0.04	0.50	0.01	4.4
Pb	9.3 ± 0.6*	9.4	0.2	0.8
Th	2.4 ± 0.1*	2.3	0.1	3.0
U	0.53 ± 0.02*	0.55	0.02	2.6

*Certificate of Analysis (U.S. Geological Survey).
†GeoReM (Geological and Environmental Reference Materials; Max Planck Institut fur Chemie, Mainz, Germany), unless otherwise noted.

Individual inclination data are provided in the Supplemental File[1].

Where inclination values are consistent, lava flows accumulated within a time frame of years to decades; otherwise, the recorded paleomagnetic character would have evolved to different values due to geomagnetic secular variation (e.g., Champion et al., 2011). This time frame coupled with the range of rates for secular variation results in single mean inclination-polarity values regardless of the specific rate of secular variation. Boundaries between magnetic groups were found to be at flow contacts and also typically within sedimentary interbeds that separate lava flows. The time break across lava flow boundaries and basalt-sediment boundaries are at least hundreds of years long, and typically much longer (e.g., Champion et al., 2011). Other than the 57 m of sediment observed between Snake River and Idaho Group basalts, there are no thick sediment horizons between individual lava flows that likely represent even longer hiatuses in volcanism, e.g., tens to hundreds of thousands of years.

Geochemical

Major Elements

Whole-rock major element compositions are listed in Table 2 (Snake River Group) and Table 3 (Idaho Group). Wendell RASA lavas are subalkaline, tholeiitic basalt (Le Maitre, 1976; Le Bas et al., 1986). Idaho Group and Snake River Group basalts have similar compositional ranges, e.g., SiO_2 = 46.0–49.0 wt%, Al_2O_3 = 12.0–16.0 wt%, FeO_t = 12.0–16.0 wt%, MgO = 7.0–10.0 wt%, CaO = 9.0–11.0 wt%, and $K_2O \leq 0.8$ wt%. Loss on ignition (LOI) is generally low for both groups; however, some samples within the Idaho Group have LOI to 2.3%.

Overall, Wendell RASA lavas define smooth to diffuse increasing and decreasing trends on MgO variation plots. TiO_2 (Fig. 3A), FeO_t (Fig. 3B), and P_2O_5 (Fig. 3D) generally increase with decreasing MgO, while SiO_2, Al_2O_3, CaO, and Cr (Fig. 3C) generally decrease with decreasing MgO. Figure 3 also demonstrates that major element compositions and trends for Wendell basalts are similar to eastern SRP tholeiitic basalts (e.g., Hughes et al., 2002). Wendell basalts, however, are higher in iron than similar basalts from the eastern SRP, but less iron rich than typical ferrobasalts often found in the western SRP. These trends have also been observed in other drill cores from the eastern SRP, e.g., WO2 and NPRE at INL (Shervais et al., 2006a), Test Area North (Geist et al., 2002a, 2002b), and USGS drill core 132 (Miller and Hughes, 2009).

Trace Elements

Trace element compositions are listed in Table 2 (Snake River Group) and Table 3 (Idaho Group). Overall, Wendell RASA lavas have trace element trends similar to basalts from the eastern SRP (Fig. 3). Although similar in general, the Snake River Group and Idaho Group demonstrate some variation, e.g., Snake River Group basalts are generally higher in Rb (Fig. 3E), Sr (Fig. 3F), Zr (Fig. 3G), and Hf (Fig. 3H) than Idaho Group basalts. These similarities and differences are best displayed on primitive mantle normalized (PM; McDonough and Sun, 1995) multielement diagrams (Fig. 4). Snake River Group basalts are heavy REE depleted (3–9× PM) compared to Idaho Group basalts (6–10.5× PM), but the light REEs are similar for both suites (20–50× PM). Snake River Group basalts have a steeper REE pattern, while Idaho Group basalts have a flatter REE pattern (Fig. 5). Both suites display similar incompatible element compositions, i.e., Ba, Pb, and Rb, to 80×, 40×, and 30× PM, respectively. The high field strength elements such as Nb, Ta, Sr, and Ti also have similar normalized concentrations, i.e., 20–40×, 20–40×, 10–20×, and 10–20× PM, respectively.

DISCUSSION

Geochemical and Time Relationships

We have used the formal group names to identify both of the >100-m-thick basalt sequences discussed herein. We introduce additional terms such as geochemical, paleomagnetic, and flow groups here. These are individual lava flows grouped together based on similar major and trace element compositions and similar inclination values, and are subgroups within the larger basalt sequences.

Stratigraphic Trends

Several trends are observed on plots of element concentration versus depth. The trends observed on these plots allow us to define 11

[1]Supplemental File. Paleomagnetic inclination data from the Wendell RASA drill core. If you are viewing the PDF of this paper or reading it offline, please visit http://dx.doi.org/10.1130/GES00914.S1 or the full-text article on www.gsapubs.org to view the Supplemental File.

TABLE 2. SNAKE RIVER GROUP BULK-ROCK ELEMENTAL ANALYSES

Flow group	1				2					3				
Flow number	1	2	3a	3b	4	5	6a	6b	7	8a	8b	9	10	11
Average depth (m)	3.1	5.5	7.7	13.5	27.4	29.4	31.2	31.5	32.3	36.3	38.9	48.8	52.2	54.6
Major elements*,†														
SiO_2	46.98	46.94	46.95	46.77	48.12	48.03	48.33	48.26	48.29	46.82	46.77	46.88	46.96	47.09
TiO_2	2.82	2.86	2.98	2.84	2.40	2.45	2.30	2.35	2.41	2.30	2.29	2.85	2.88	2.89
Al_2O_3	14.83	14.63	14.53	14.54	15.27	15.12	15.53	15.37	15.36	15.35	15.03	14.55	14.65	14.58
FeO_t	14.7	14.75	14.98	14.77	13.62	13.78	13.3	13.48	13.52	13.93	13.99	14.99	14.97	15.01
MnO	0.17	0.17	0.18	0.18	0.16	0.16	0.16	0.16	0.16	0.17	0.17	0.18	0.18	0.18
MgO	8.0	8.16	7.76	8.15	8.03	8.17	7.95	8.04	7.82	9.06	9.55	8.23	7.89	7.73
CaO	9.35	9.37	9.44	9.40	9.69	9.60	9.7	9.62	9.69	9.75	9.65	9.69	9.73	9.68
Na_2O	2.52	2.49	2.48	2.77	2.32	2.28	2.35	2.32	2.34	2.31	2.28	2.17	2.24	2.28
K_2O	0.52	0.51	0.55	0.52	0.43	0.44	0.43	0.44	0.45	0.34	0.31	0.36	0.40	0.43
P_2O_5	0.62	0.62	0.65	0.63	0.41	0.42	0.4	0.41	0.41	0.41	0.40	0.51	0.54	0.57
LOI	–0.72	–0.87	–0.76	–0.86	–0.56	–0.45	–0.38	–0.44	–0.49	–0.57	–0.65	–0.65	–0.67	–0.69
Mg#	51.9	52.3	50.7	52.2	53.9	54.0	54.2	54.1	53.4	56.3	57.5	52.1	51.1	50.5
Cr	240.6	237.0	225.8	245.5	247.4	256.9	233.6	235.5	224.2	248.5	252.8	243.4	233.3	218.0
K	4309	4255	4579	4326	3582	3671	3581	3653	3747	2837	2602	3006	3332	3534
P	2693	2710	2845	2747	1798	1844	1754	1792	1799	1790	1753	2221	2350	2506
Trace elements§														
La	28.1	25.9	30.3	28.8	22.0	20.0	21.8	23.8	24.2	11.3	12.7	23.9	24.5	27.5
Ce	61.4	56.4	65.9	63.0	47.7	44.5	48.8	51.6	47.7	30.0	30.9	53.8	55.2	61.5
Pr	8.2	7.5	8.8	8.4	6.3	5.9	6.5	6.8	7.0	3.7	4.0	7.2	7.4	8.3
Nd	35	33	37	36	27	26	28	29	30	16	18	32	33	36
Sm	7.7	7.4	8.2	8.0	6.2	6.0	6.3	6.6	6.9	3.6	4.3	7.1	7.3	8.1
Eu	2.70	2.61	2.89	2.81	2.22	2.13	2.23	2.38	2.46	1.26	1.55	2.54	2.63	2.86
Gd	10.09	9.51	11.30	10.90	8.60	7.67	8.47	9.06	9.77	4.51	5.28	9.50	9.62	10.83
Tb	1.44	1.28	1.60	1.54	1.23	1.06	1.21	1.31	1.40	0.62	0.71	1.32	1.34	1.49
Dy	8.09	7.45	8.90	8.54	6.94	6.23	6.70	7.33	7.86	3.41	4.24	7.34	7.49	8.28
Ho	1.63	1.44	1.78	1.70	1.39	1.21	1.35	1.48	1.59	0.67	0.81	1.46	1.49	1.65
Er	4.5	4.2	5.0	4.7	3.9	3.5	3.7	4.2	4.5	1.8	2.4	4.1	4.1	4.6
Tm	0.62	0.54	0.68	0.64	0.53	0.45	0.51	0.57	0.61	0.23	0.30	0.55	0.55	0.62
Yb	4.0	3.7	4.3	4.1	3.5	3.0	3.2	3.6	3.9	1.4	2.0	3.5	3.5	3.9
Lu	0.58	0.51	0.63	0.60	0.50	0.42	0.46	0.53	0.57	0.19	0.28	0.51	0.50	0.56
Sc	31.3	28.1	34.2	20.4	32.5	22.0	24.1	34.7	33.6	35.4	24.1	31.5	19.4	32.7
Rb	16	14	16	14	13	12	13	15	14	13	9	10	8	12
Sr	306	300	307	287	301	288	286	336	332	314	275	287	226	321
Y	38	30	39	29	33	23	24	37	29	32	18	34	26	41
Zr	283	257	292	274	220	210	217	246	237	203	158	261	193	312
Nb	25.4	23.3	26.0	24.2	19.6	18.3	18.4	25.7	19.7	21.9	12.0	27.0	22.3	32.6
Ba	472	445	485	449	388	379	367	409	382	332	293	321	390	387
Hf	6.4	5.8	6.6	6.2	5.4	5.0	5.2	5.7	5.8	4.4	5.2	5.3	5.1	6.3
Ta	1.57	1.44	1.56	1.41	1.15	1.11	1.05	1.57	1.23	1.34	1.48	1.51		1.83
Th	1.8	1.5	1.8	1.0	1.6	1.0	1.1	2.0	1.9	1.3	1.3	1.0		1.3
U	0.54	0.45	0.52	0.49	0.43	0.39	0.42	0.50	0.49	0.40	0.40	0.32		0.40
V	293	288	314	288	290	302	286	315	311	304	424	297	296	318
Pb	3.6	2.6	0.7	0.7	0.1	0.7	8.4	3.5	4.3	4.6	5.2	3.2		3.7

(*continued*)

geochemical groups (Fig. 5). Within the Snake River Group, there are series of near-surface lavas that have higher SiO_2 (49.0 wt%) than the rest of the group, which averages ~48.0 wt% (Fig. 5B). K_2O, in general, increases upsection from ~0.4 to 0.52 wt% (Fig. 5D). TiO_2 displays a wide range in composition, and is group dependent, e.g., groups 1 and 2 have nearly constant compositions, ~2.8 and 2.4 wt%, on average, group 3 ranges from 2.3 to 2.9 wt%, group 4 ranges from 2.4 to 2.5 wt%, and group 5 ranges from 2.9 to 3.4 wt% (Fig. 5E). Chromium is ~250 ppm, on average, for groups 1, 2, and 3, however, it ranges from 230 to 280 ppm for group 4 and 150 to 260 ppm for group 5 (Fig. 5F). Within the Idaho Group, SiO_2 generally increases from ~46.0 wt% near the base to 48.0 wt% near the top (Fig. 5B). K_2O displays a wide range within this group, i.e., 0.1–0.4 wt%, excluding the ash unit (Fig. 5D). TiO_2 in groups 6 and 8 averages ~2.8 wt%, while in other groups has wide ranges, e.g., group 7, 2.3–2.7 wt%; group 9, 2.4–2.8 wt%; group 10, 2.4–3.1 wt%; and group 11, 2.1–2.6 wt%. Chromium below the 250 mbs ash decreases upsection from 350 to 200 ppm; above this horizon, chromium decreases upsection from 400 to 250 ppm (Fig. 5F).

Based on this chemical stratigraphy, the 11 geochemical groups are also classified as fractionation (decreasing MgO and increasing TiO_2 upsection), recharge (increasing MgO and decreasing TiO_2 upsection), or neither (Fig. 5C). This well includes five fractionation trends (4, 5, 7, 8, and 10), two recharge trends (3 and 11), and three groups that do neither (1, 2, and 9). Group 6 is a possible recharge trend, consistent with TiO_2 data, although there were only 2 flows available for sampling. Flow 16a is grouped with group 5, while flow 16b is grouped with group 4. This determination was made by compositions shown in Table 2 (especially FeO_t and TiO_2) and by the depth-chemistry trends shown in Figure 5. We explore this occurrence further.

Correlation of Paleomagnetic and Geochemical Groups

The Snake River Group was divided into five geochemical groups. Groups 1 and 2 are separated by distinct paleomagnetic mean inclination values. Group 1, with mean inclination of 74°, and group 2, with mean inclination of 59°, are separated by at least centuries. These two units are therefore manifestations of two separate

TABLE 2. SNAKE RIVER GROUP BULK-ROCK ELEMENTAL ANALYSES (*continued*)

Flow group	4				5										
Flow number	12	13	14	16b	15a	15b	16a	17	18	19	20	21a	21b	22	23
Average depth (m)	59.7	61.8	67.3	85.8	74.8	75.5	79.6	94.2	96.4	98.1	100.3	107.0	109.4	112.3	116.1
Major elements*,†															
SiO_2	47.01	47.12	47.14	47.13	46.61	46.55	46.68	46.53	47.04	46.99	46.89	46.92	46.85	46.89	46.91
TiO_2	2.87	2.90	2.71	2.52	3.41	3.36	3.17	3.32	3.09	3.04	3.11	2.93	2.90	2.99	2.95
Al_2O_3	14.68	14.56	14.68	15.15	14.13	14.34	14.57	14.09	14.42	14.70	14.34	14.49	14.58	14.43	14.35
FeO_t	14.93	15.02	14.70	13.99	16.42	16.34	16.17	16.10	15.59	15.39	15.61	15.41	15.54	15.44	15.50
MnO	0.18	0.18	0.17	0.16	0.19	0.19	0.18	0.19	0.18	0.18	0.18	0.18	0.18	0.18	0.18
MgO	7.80	7.74	8.12	8.48	6.81	6.90	7.00	7.51	7.32	7.20	7.54	7.80	7.67	7.69	7.89
CaO	9.73	9.67	9.77	9.87	9.20	9.19	9.11	9.53	9.57	9.66	9.54	9.51	9.52	9.60	9.48
Na_2O	2.27	2.25	2.21	2.25	2.35	2.34	2.38	2.21	2.28	2.38	2.27	2.27	2.28	2.27	2.24
K_2O	0.40	0.43	0.39	0.42	0.53	0.50	0.48	0.38	0.38	0.39	0.40	0.38	0.39	0.40	0.38
P_2O_5	0.56	0.57	0.52	0.45	0.80	0.76	0.75	0.56	0.56	0.55	0.55	0.54	0.54	0.55	0.55
LOI	–0.74	–0.63	–0.47	–0.56	–0.68	–0.73	–0.65	–0.68	–0.32	–0.44	–0.74	–0.61	–0.64	–0.67	–0.64
Mg#	50.9	50.5	52.2	54.5	45.1	45.6	46.2	48.0	48.2	48.1	48.9	50.1	49.4	49.7	50.2
Cr	230.1	224.1	251.1	282.4	156.6	162.8	162	226	219.1	201.6	232.0	246.0	236.0	240.7	264.8
K	3345	3585	3274	3510	4437	4156	4000	3180	3191	3197	3335	3187	3241	3327	3195
P	2445	2485	2281	1974	3499	3299	3262	2443	2452	2414	2395	2363	2343	2405	2412
Trace elements§															
La	23.0	23.1	23.9	14.4	29.8	23.6	24.1	16.2	15.7	13.4	15.1	17.3	14.5	21.4	18.3
Ce	50.2	54.9	53.8	35.4	70.2	61.5	63.3	42.7	40.1	36.1	41.3	43.0	39.7	50.7	44.5
Pr	6.9	6.9	6.9	4.6	8.3	6.8	6.9	5.2	5.1	4.2	4.9	5.3	4.5	7.0	5.6
Nd	30	31	34	21	36	29	29	23	23	19	22	25	19	32	25
Sm	6.7	6.8	7.9	4.9	7.6	6.2	5.9	5.1	5.1	4.1	4.9	5.6	4.3	7.4	5.5
Eu	2.40	2.30	2.50	1.81	2.56	2.14	2.00	1.85	1.84	1.51	1.78	2.07	1.53	2.52	2.03
Gd	9.05	7.30	9.10	5.85	9.07	7.81	7.29	6.00	5.64	4.59	5.52	6.44	4.65	8.11	5.82
Tb	1.27	1.04	1.10	0.79	1.15	1.07	0.96	0.82	0.79	0.62	0.76	0.84	0.63	1.16	0.87
Dy	7.09	5.90	7.30	4.72	6.57	5.76	5.09	4.56	4.31	3.37	4.17	4.98	3.40	6.63	5.11
Ho	1.40	1.20	1.30	0.89	1.19	1.14	0.98	0.88	0.84	0.65	0.81	0.92	0.66	1.33	0.98
Er	3.9	3.20	4.1	2.6	3.5	3.2	2.7	2.4	2.3	1.8	2.2	2.7	1.8	3.7	2.7
Tm	0.53	0.40	0.51	0.32	0.42	0.41	0.35	0.31	0.29	0.22	0.29	0.33	0.23	0.50	0.35
Yb	3.4	3.6	3.6	2.2	2.8	2.6	2.1	1.9	1.8	1.3	1.8	2.2	1.4	3.2	2.3
Lu	0.48	0.40	0.40	0.30	0.38	0.37	0.29	0.26	0.24	0.18	0.24	0.29	0.19	0.47	0.31
Sc	30.8	30.1	31.8	22.8	28.3	34.1	31.3	38.1	41.3	33.9	37.8	18.3	37.3	29.8	26.7
Rb	11	12	8	10	12	13	12	11	14	11	13	7	13	8	10
Sr	292	320	275	307	347	363	373	361	397	341	363	281	353	280	303
Y	37	31	27	19	38	47	37	36	48	31	44	20	43	27	28
Zr	265	298	267	183	339	377	358	330	346	273	311	233	305	268	247
Nb	26.9	22.0	18.7	13.3	39.1	47.5	33.5	22.7	34.2	20.4	30.1	17.2	30.2	17.9	17.8
Ba	353	388	387	346	489	486	480	428	512	413	461	385	425	417	375
Hf	5.5	6.2	5.9	4.3	7.2	7.5	7.7	7.2	7.4	6.2	6.9	5.3	6.3	6.2	5.8
Ta	1.56	1.29	1.10	0.85	2.16	2.52	2.01	1.47	2.09	1.28	1.93	1.08	1.78	1.10	1.11
Th	1.2	1.3	1.1	0.8	1.5	1.7	1.7	1.7	1.9	1.4	1.7	0.8	1.6	1.3	1.4
U	0.34	0.39	0.30	0.27	0.46	0.52	0.49	0.48	0.54	0.42	0.49	0.33	0.48	0.40	0.42
V	280	333	302		342	339	297	392	381	319	364		342	311	324
Pb	3.3	3.7			5.2	5.2	5.0	4.4	5.0	3.9	4.5		4.1		3.7

Note: Major oxides are in weight percent; trace elements and rare earth elements are in parts per million. LOI—loss on ignition. Flow groups as in text.
*Measured by X–ray fluorescence.
†Normalized to 100 wt% on a volatile-free basis.
§Measured by inductively coupled plasma–mass spectrometer.

batches of magma coming to the surface at two different times. Groups 3 and 4 have a boundary at ~58 m, which is in the middle of a consistent (77° ± 1°) normal polarity interval, probably emplaced over a short time span, i.e., a few years to decades. Group 3, based on chemistry, is a recharge cycle; however, the first 2 lava flows from group 3 occur within lavas having a mean inclination value of 71° ± 3°, shallower than the rest of group 3 lava flows, and could represent a hiatus of a century or two. Paleomagnetic data suggest that groups 4 and 3 together represent a fractionation-recharge episode of limited time duration. The mean inclination value of 76° ± 3° for the top part of group 5 could be paleomagnetically associated with the short time interval of groups 3 and later group 4, but Figure 5 does not suggest any associated trends. In addition, the top part of group 5 is separated from the top part of group 4 by a sedimentary interbed at 73.5 mbs, and is thus time independent, and only coincidentally similar in mean inclination value. The upper part of group 5 is separated from its lower part by a singular lava flow (flow 16b) from group 4. This section has a mean inclination value of 52° ± 6°, completely different from both the lower group 5 mean inclination of 75° ± 1° and the upper part of group 5 mean inclination of 76° ± 3°. The time frame to move from 75° to 52° has to be viewed as at least several centuries, but could range from thousands to tens of thousands of years. Similarly, the time frame to move from 52° back to 76° is an additional several centuries to many thousands of years. Therefore, the overall time frame from the bottom of group 5 to the top of group 4 has to be considered close to a thousand years, but possibly very much longer.

Groups 4 and 5 are the only flow groups in this core that stratigraphically overlap or interleave, and from the paleomagnetic data, cross over four different time periods. This finding is of particular interest because no other SRP drill core rocks have been shown to exhibit this behavior. Our interpretation is that two vents were concurrently active. Alternatively, this chemical stratigraphy could represent an evolving magma chamber, giving rise to multiple

TABLE 3. IDAHO GROUP BULK-ROCK ELEMENTAL ANALYSES

Flow group	6		7				8				Ash unit	9					
Flow number	25	26	27	28	29	30	31	32	33a	33b		34	35	36	37	38	40
Average depth (m)	187.7	196.5	212.0	215.1	223.9	227.9	229.7	232.4	238.0	242.2	251.4	252.9	254.9	257.9	259.4	262.3	262.9
Major elements*,†																	
SiO_2	47.41	47.50	46.98	47.36	47.34	47.32	46.46	46.26	46.81	46.72	58.20	46.51	47.35	47.03	47.11	46.96	46.98
TiO_2	2.45	2.55	2.68	2.55	2.42	2.37	2.79	2.61	2.59	2.64	1.99	2.84	2.60	2.63	2.63	2.82	2.44
Al_2O_3	15.31	15.16	15.09	15.12	15.04	15.23	14.35	14.37	14.66	14.47	18.70	14.87	15.02	15.09	15.01	14.53	15.27
FeO_t	13.93	14.29	14.73	14.30	14.21	14.13	14.91	14.53	14.30	14.45	11.27	15.75	15.03	15.29	15.32	15.64	14.96
MnO	0.17	0.17	0.18	0.17	0.15	0.15	0.18	0.17	0.17	0.16	0.16	0.19	0.13	0.18	0.18	0.19	0.17
MgO	8.22	7.88	7.97	7.98	8.78	8.91	8.57	8.87	8.90	9.19	3.20	7.40	8.02	7.38	7.32	7.48	8.01
CaO	10.16	10.08	10.19	10.19	10.00	9.83	10.20	10.76	10.08	10.12	3.74	9.75	9.56	9.55	9.54	9.44	9.39
Na_2O	2.11	2.13	2.02	2.02	2.07	2.03	2.03	1.99	2.13	2.00	1.17	2.30	2.14	2.41	2.37	2.35	2.34
K_2O	0.27	0.26	0.11	0.11	0.01	0.03	0.25	0.23	0.20	0.03	1.40	0.29	0.06	0.40	0.43	0.47	0.41
P_2O_5	0.36	0.39	0.43	0.43	0.37	0.37	0.63	0.58	0.57	0.58	0.42	0.55	0.51	0.52	0.52	0.59	0.49
LOI	–0.36	0.01	0.28	–0.49	2.15	2.29	–0.21	0.16	–0.48	–0.48	6.95	–0.03	3.9	–0.18	0.02	–0.44	–0.41
Mg#	53.9	52.2	51.7	52.5	55.0	55.6	53.2	54.7	55.2	55.7	36.0	48.2	51.4	48.9	48.6	48.6	51.5
Cr	269.2	262.1	253.1	276.7	311.9	316.0	379.8	403.1	398.4	391.2	72.7	214.5	233.0	214.2	219.1	199.5	229.6
K	2204	2119	893	2524	82	247	2040	1869	1627	245	11621	2441	493	3346	3590	3896	3416
P	1588	1714	1877	1755	1631	1603	2746	2521	2481	2538	1833	2396	2205	2274	2274	2561	2138
Trace elements§																	
La	14.8	19.9	31.2	23.0	16.3	15.5	22.7	20.1	20.7	22.9	27.3	27.7	25.6	28.3	26.1	33.2	21.0
Ce	35.3	48.2	70.4	53.4	37.5	37.5	54.8	46.2	49.8	52.6	57.4	61.7	56.4	61.9	61.2	73.1	47.8
Pr	4.8	6.8	10.1	7.4	4.9	5.2	7.5	6.2	6.7	7.2	7.7	8.4	7.5	8.3	8.1	9.9	6.4
Nd	23	31	46	34	26	25	34	31	31	33	34	36	33	36	36	44	29
Sm	5.6	7.6	11.3	8.2	6.2	6.0	7.9	7.4	7.1	7.6	7.9	8.4	5.0	8.4	8.3	10.1	6.7
Eu	1.98	2.65	3.89	2.85	1.92	2.11	2.67	2.22	2.41	2.60	2.04	2.79	5.17	2.80	2.68	3.24	2.27
Gd	6.34	8.00	12.31	8.83	7.61	6.66	7.82	8.61	7.03	9.93	8.91	11.23	8.88	11.12	8.17	10.36	7.35
Tb	0.90	1.21	1.87	1.34	1.01	0.96	1.14	1.10	1.02	1.39	1.22	1.62	1.35	1.61	1.21	1.52	1.02
Dy	5.56	7.22	11.08	7.96	6.80	5.86	6.64	7.31	6.07	7.95	7.71	9.11	8.06	9.06	7.29	9.09	6.19
Ho	1.08	1.46	2.26	1.63	1.20	1.13	1.31	1.32	1.20	1.57	1.44	1.86	1.60	1.85	1.44	1.83	1.20
Er	3.2	4.1	6.4	4.6	3.93	3.4	3.6	4.1	3.3	4.5	4.61	5.2	4.5	5.2	4.1	5.2	3.5
Tm	0.41	0.55	0.89	0.65	0.91	0.43	0.49	0.53	0.44	0.60	0.64	0.71	0.61	0.72	0.56	0.71	0.45
Yb	2.8	3.6	5.8	4.2	3.60	2.9	3.1	3.6	2.8	3.9	4.2	4.6	4.1	4.7	3.6	4.7	3.1
Lu	0.39	0.52	0.85	0.60	0.44	0.41	0.45	0.41	0.39	0.56	0.61	0.66	0.57	0.68	0.50	0.68	0.42
Sc	28.3	39.0	49.1	36.9	33.3	20.9	48.7	31.9	35.9	29.5	19.4	36.6	28.5	31.1	44.7	34.6	23.2
Rb	7	10	7	10	3	2	10	5	8	3	45	10	7	13	17	13	10
Sr	233	273	344	256	181	228	357	183	285	258	249	269	264	273	332	274	259
Y	22	33	43	30	26	19	43	27	32	32	28	45	32	45	45	39	24
Zr	159	205	273	197	183	156	331	215	234	228	212	249	219	248	301	267	188
Nb	12.1	15.6	20.8	15.1	13.1	11.9	23.7	14.8	17.8	18.2	20.2	23.3	19.1	23.4	26.1	23.2	16.5
Ba	294	340	400	303	222	238	389	240	280	286	727	436	318	477	503	381	350
Hf	4.0	5.3	7.2	5.0	4.5	3.9	7.2	2.9	5.7	5.4	5.9	6.5	5.4	6.2	7.4	6.5	4.6
Ta	0.80	1.01	1.50	0.97	0.82	0.77	1.52	0.94	1.15	1.14	1.31	1.54	1.18	1.42	1.64	1.39	0.99
Th	0.8	1.4	1.8	1.3	1.2	0.7	1.7	1.1	1.3	1.1	5.0	2.1	1.6	2.0	2.5	2.1	1.1
U	0.25	0.37	0.45	0.35	0.3	0.29	0.50	0.3	0.37	0.33	1.12	0.49	0.45	0.55	0.67	0.57	0.37
V		348	445	306	307		421	282	331	320		342	294	314	425	347	
Pb		3.4	4.1	3.3			4.7		4.1	1.6		2.1	3.2	1.4	5.6	5.2	

(*continued*)

vents, or the reversal may represent tapping of a new magma storage chamber, or nonuniform distribution of the erupted lava. These interpretations are unsatisfactory because the three lava flows that overlie flow 16b (~86.0 mbs) continue the fractionation trend observed from the lower part of group 4. The three lava flows that compose the upper part of group 5 continue the fractionation trend observed in the lower part of group 5. In these other proposed scenarios, the continuation of these trends would be considered coincidences. In addition, the magma chamber would require complete overturn in the magma supply, in order to erupt the primitive-like compositions observed in flow 16b (Table 2) and completely overwhelm remnants of magma from the previous fractionation cycle.

Idaho Group basalts were divided into six geochemical groups. Groups 6 and 7 are separate parts of a consistent (–71° ± 1°) reversed inclination interval, lasting ~100 yr. Groups 8 and 9 have a mean inclination of –68° ± 2°; however, group 9 is separated from groups 6, 7, and 8 by the 250 mbs ash unit. Two lines of evidence support the conclusion that groups 9 through 6 erupted in ~100 yr: (1) the consistent steep reversed inclinations, and (2) the ash between groups 8 and 9 may be an indication of an instantaneous event; if so, groups 8 and 9 would be considered a recharge period, followed by fractionation and weak recharge (i.e., groups 6–8). However, if the ash between groups 8 and 9 is on a long-term surface, the groups 6–8 sequence represents fractionation followed by weak recharge, and group 9 is an earlier unrelated event. The reversal in polarity between groups 9 and 10 is an indication that they are separated by at least several thousands, if not tens of thousands, of years. Groups 10 and 11 are separated based on chemistry into a recharge cycle, followed by a fractionation cycle. However, they record a consistent mean normal polarity inclination value (67° ± 1°). These two flow groups occur within an ~50-m-thick package of massive basalt that, based on paleomagnetism, represents a single eruption cycle requiring at most a few decades to erupt and be emplaced. It is difficult to imagine that the fractionation-recharge cycles represented by groups 10 and 11 originated from one vent. It seems more likely that these two cycles erupted from different vents, each with its own plumbing system that erupted unrelated lavas

TABLE 3. IDAHO GROUP BULK-ROCK ELEMENTAL ANALYSES (*continued*)

Flow group	10									11						
Flow number	41	43	44	45	47	48	49	50a	50b	51a	51b	52a	52b	52c	52d	52e
Average depth (m)	266.4	267.4	268.2	271.0	274.4	276.8	279.8	283.0	285.9	293.3	297.7	301.8	305.9	314.5	321.5	322.4
Major elements*,†																
SiO_2	46.51	46.91	46.57	46.76	46.95	46.73	46.66	46.77	46.74	46.99	47.01	46.74	47.08	46.93	46.86	46.10
TiO_2	2.41	2.64	3.07	2.47	2.84	3.15	2.59	2.56	2.59	2.15	2.18	2.34	2.26	2.24	2.56	2.42
Al_2O_3	15.44	14.99	14.15	15.49	14.97	14.23	15.07	15.02	15.03	15.18	15.10	15.03	15.15	14.95	14.97	14.79
FeO_t	13.98	14.82	15.54	14.27	15.23	15.83	14.79	14.78	14.78	13.70	13.81	14.26	13.79	13.86	14.79	15.27
MnO	0.17	0.18	0.2	0.18	0.18	0.19	0.17	0.17	0.17	0.17	0.17	0.17	0.16	0.17	0.17	0.17
MgO	8.04	7.5	6.88	7.97	7.22	7.1	8.41	8.44	8.40	9.31	9.16	8.95	9.16	9.18	8.46	8.56
CaO	11.25	10.53	11.19	10.65	10.19	10.29	9.89	9.83	9.83	10.32	10.35	10.24	10.33	10.50	9.77	10.43
Na_2O	2.00	2.07	2.07	2.00	2.02	2.02	2.20	2.20	2.23	2.04	2.11	2.10	2.04	2.07	2.21	2.11
K_2O	0.14	0.21	0.16	0.13	0.24	0.28	0.2	0.22	0.22	0.15	0.14	0.17	0.02	0.09	0.18	0.16
P_2O_5	0.43	0.56	0.56	0.45	0.53	0.56	0.44	0.43	0.43	0.35	0.37	0.40	0.38	0.38	0.43	0.39
LOI	0.24	–0.35	–0.20	–0.03	–0.23	–0.34	–0.66	–0.69	–0.74	–0.60	–0.56	0.83	0.39	0.12	1.29	–0.30
Mg#	53.2	50.1	46.7	52.5	48.4	47.0	53.0	53.1	53.0	57.4	56.8	55.4	56.8	56.8	53.1	52.6
Cr	227.1	209.9	236.3	230.1	229.5	237.7	269.5	271.7	262.0	349.3	353.7	316.5	346.9	348.1	270.2	247.7
K	1152	1709	1311	1065	1974	2295	1627	1866	1862	1218	1133	1397	163	747	1483	1304
P	1860	2438	2455	1981	2292	2456	1925	1877	1872	1537	1617	1729	1672	1659	18.62	1714
Trace elements§																
La	19.1	22.1	31.4	19.4	25.3	24.7	21.7	16.2	25.9	12.8	19.0	19.7	17.0	13.5	21.9	18.6
Ce	43.2	50.4	72.7	44.4	57.2	56.5	48.9	36.7	58.1	29.4	42.8	44.7	38.7	31.0	49.1	42.4
Pr	6.1	7.0	10.0	6.2	7.9	7.8	6.8	5.0	8.0	4.0	5.9	6.1	5.3	4.2	6.8	5.8
Nd	28	33	46	29	35	35	30	24	36	20	26	27	24	20	30	26
Sm	2.5	7.9	4.0	2.5	8.5	8.4	2.5	5.9	4.6	4.9	2.3	4.3	2.1	5.0	2.5	6.3
Eu	6.88	2.76	11.40	6.88	2.99	2.86	7.25	2.01	7.39	1.69	6.47	4.60	6.01	1.72	7.33	2.22
Gd	7.29	10.30	12.37	7.37	11.60	8.98	7.94	7.25	10.21	5.91	7.18	7.23	6.59	6.11	7.79	8.58
Tb	1.21	1.46	2.01	1.23	1.69	1.41	1.33	0.98	1.66	0.82	1.19	1.18	1.08	0.84	1.30	1.27
Dy	7.72	8.73	12.53	7.58	9.58	8.72	8.30	6.28	10.18	5.43	7.47	7.31	6.95	5.49	8.05	7.37
Ho	1.54	1.73	2.52	1.52	1.94	1.71	1.66	1.17	2.07	1.02	1.50	1.47	1.41	1.02	1.63	1.52
Er	4.3	5.1	7.0	4.2	5.4	4.8	4.7	3.7	5.9	3.2	4.2	4.2	4.0	3.2	4.5	4.3
Tm	0.57	0.66	0.94	0.56	0.75	0.64	0.64	0.44	0.80	0.39	0.58	0.58	0.54	0.39	0.61	0.60
Yb	3.9	4.5	6.4	3.9	4.8	4.3	4.3	3.2	5.4	2.9	4.0	3.9	3.7	2.9	4.2	3.9
Lu	0.55	0.64	0.90	0.53	0.70	0.59	0.61	0.43	0.76	0.39	0.56	0.54	0.51	0.39	0.59	0.57
Sc	39.1	29.6	62.8	35.7	35.9	34.6	37.6	28.4	59.0	28.5	39.7	37.3	44.6	24.5	36.5	32.9
Rb	6	6	8	6	9	8	8	8	12	6	7	7	2	3	8	10
Sr	256	238	317	258	274	256	264	240	374	205	236	242	222	144	271	239
Y	30	32	49	29	43	35	32	24	45	20	30	30	27	20	32	35
Zr	200	232	329	196	254	261	203	176	278	148	179	183	169	155	204	182
Nb	14.7	16.6	23.8	14.3	20.4	18.4	17.2	14.4	22.5	11.8	14.0	14.8	13.4	12.5	16.6	16.1
Ba	266	330	431	265	403	317	241	229	335	198	221	227	198	182	244	248
Hf	5.0	5.4	8.0	4.9	6.4	6.0	5.5	4.2	7.0	3.6	4.5	4.6	4.2	3.8	5.1	4.5
Ta	1.00	1.03	1.60	0.95	1.33	1.18	1.25	0.91	1.53	0.75	0.94	0.96	0.86	0.79	1.10	1.00
Th	1.0	0.9	1.7	1.1	1.5	1.6	1.7	1.1	2.1	0.8	1.4	1.5	1.3	0.8	1.6	1.4
U	0.28	0.30	0.45	0.29	0.43	0.40	0.42	0.31	0.55	0.25	0.33	0.36	0.37	0.28	0.44	0.37
V	333	347	549	297	333	362	351		533		314	331	346		364	307
Pb	3.1	2.1	4.8		1.2	4.2	4.0		5.5		3.5	3.9	3.3		4.6	

Note: Major oxides in weight percent; trace elements and rare earth elements in parts per million. LOI—loss on ignition. Flow groups as in text.
*Measured by X-ray fluorescence.
†Normalized to 100 wt% on a volatile-free basis.
§Measured by inductively coupled plasma–mass spectrometer.

during nearly simultaneous eruptions. Based on the consistency of the intra–lava flow inclination values, Idaho Group lava flows must have erupted within only months to decades, with a maximum of ~100 yr; eruptions that last longer than 100 yr generally will not preserve the same paleomagnetic inclination (Champion et al., 2002, 2011).

Wendell Chronostratigraphy

Most of the surface of the central SRP is covered with normal-magnetic-polarity basalts, erupted during the C1n Brunhes Normal Polarity Chron, which has been dated as younger than 781 ka (Gradstein et al., 2005). Lava flows within the Snake River Group are thought to be younger than 400 ka, based on inclination correlation to nearby surface outcrops and $^{40}Ar/^{39}Ar$ dating (Tauxe et al., 2004). With ~120 m of basalt in the Snake River Group, this suggests an emplacement rate of ~30 m/100 k.y. This emplacement rate agrees with the range in emplacement rates observed at INL drill cores, i.e., 16–67 m/100 k.y. (Champion et al., 2002).

The two sediment units offer additional clues into the chronostratigraphy of this well. Both sediment intervals (122.8–179.8 m and 325.0–340.0 m) are thought to be equivalent in age with the Glenns Ferry Formation (ca. 4.0–3.2 Ma: Hart and Brueseke, 1999; Link et al., 2002; Kauffman and Othberg, 2004; Ruez, 2009). The top of the sediment interval between Snake River and Idaho Group basalts contains gravels and conglomerates with clasts of rhyolite. This section is comparable to the late Pliocene Tuana Gravel (ca. 2.5 Ma; Sadler and Link, 1996; Link et al., 2002; Beranek et al., 2006). The Tuana Gravel is interpreted to represent several cycles of progradation and also contains clasts of rhyolite. In other places in the central SRP, the Tuana Gravel has been found to unconformably overlie the uppermost Glenns Ferry Formation (Beranek et al., 2006). Detrital zircon populations from the middle sediment unit are as young as 3.5 Ma (sample I.67PL05 from Hodges et al., 2009), while detrital zircon populations from the lower sediments are as young as 7.1 Ma (sample J.68PL05 from Hodges et al.,

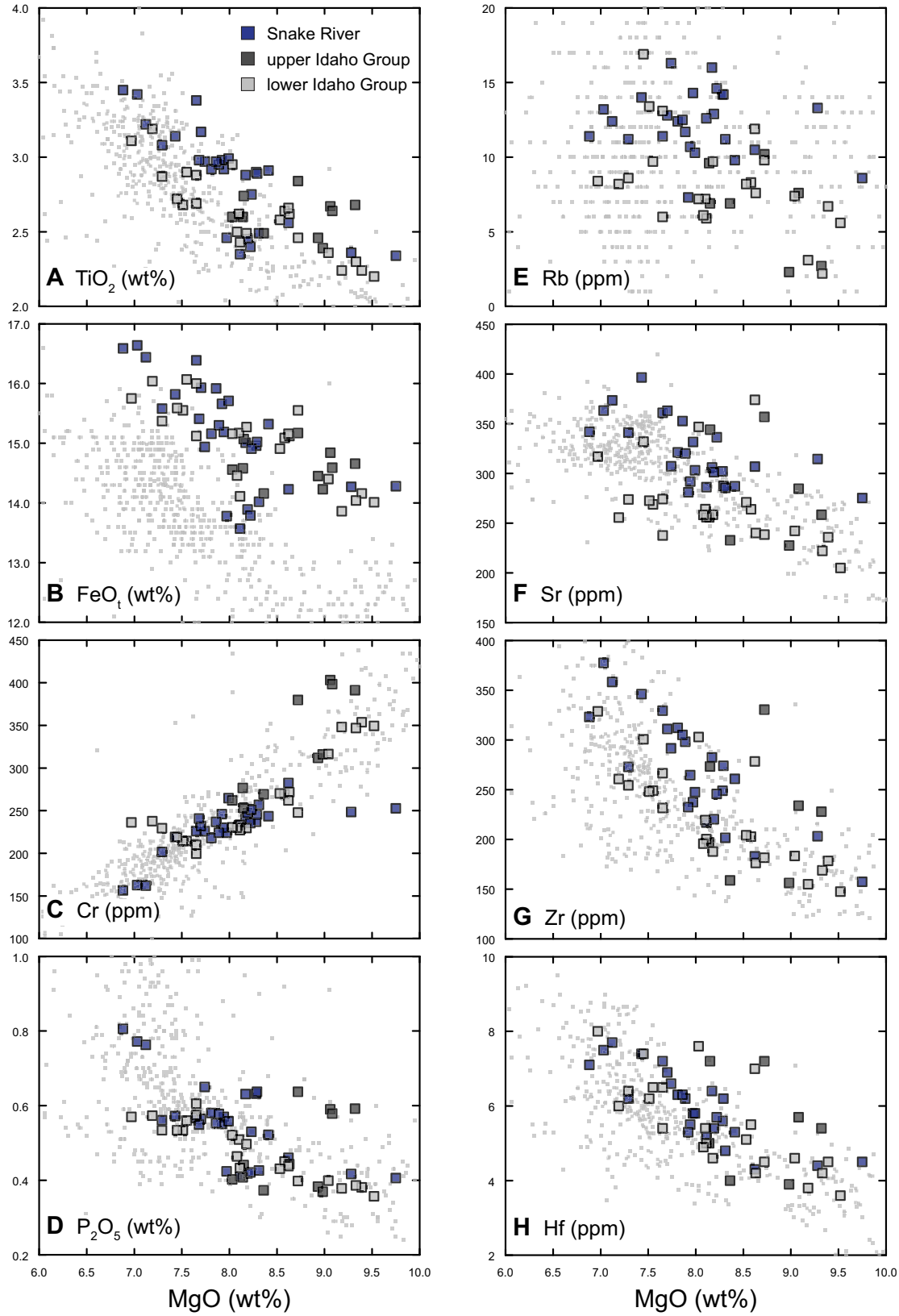

Figure 3. Selected major and trace element compositions of Wendell Regional Aquifer Systems Analysis (RASA) basalts compared to eastern Snake River Plain (ESRP) olivine tholeiites (Hughes et al., 2002). Snake River Group basalts are shown in blue squares, upper Idaho Group basalts are shown in dark gray squares, lower Idaho Group basalts are shown in light gray squares, and ESRP olivine tholeiites are shown in small gray squares.

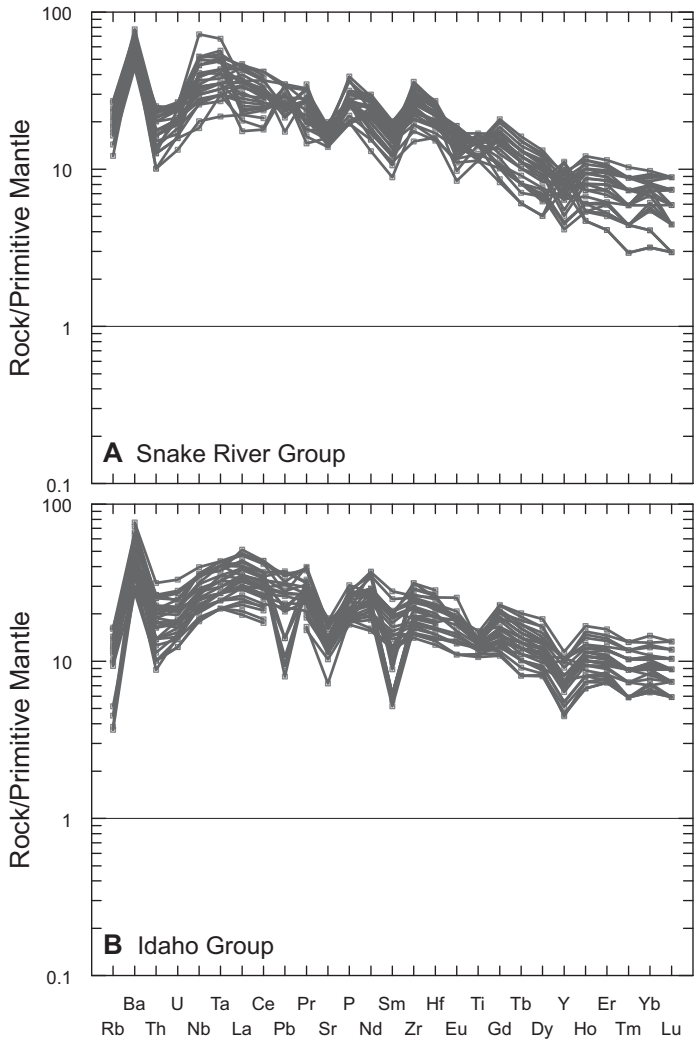

Figure 4. Primitive mantle normalized (McDonough and Sun, 1995) multielement spider diagrams. (A) Snake River Group. (B) Idaho Group basalts. Trace elements are arranged in order of decreasing compatibility from right to left.

2009). These zircons probably record drainage from the paleo–Wood and Lost River systems; the zircons were likely sourced from the 3–6 Ma Magic Reservoir volcanic field (Honjo et al., 1992) and the 8–12 Ma central SRP rhyolites exposed in the Mount Bennett Hills and Lake Hills (Oakley and Link, 2006), respectively; both are north-northeast of Wendell (Hodges et al., 2009).

Hart and Brueseke (1999) and Link et al. (2002) chronicled similar strata of basalt and sediments at Hagerman Fossil Beds National Monument and proposed an early to mid-Blancan age (North American Land Mammal Age). The emplacement of the entire Idaho Group could therefore be bracketed from ca. 2.5 to 4.0 Ma. One key feature from this section is the change from normal polarity in the lower Idaho Group to reversed polarity in the upper Idaho Group. Multiple normal-reverse chron packages are within the Blancan mammal age. We propose two plausible scenarios: the reverse-polarity upper Idaho Group represents ≤100 yr of the lower Gilbert Chron (C2Ar), and the normal-polarity lower Idaho Group represents ≤100 yr of the C3n.1n Cochiti subchron; alternatively, these lavas erupted exclusively within the Gauss (C2An) Chron, with the reverse-polarity upper Idaho Group representing ≤100 yr of the C2An.3n subchron, and the normal-polarity lower Idaho Group representing ≤100 yr of the Mammoth subchron (Gradstein et al., 2005). Additional time constraints on the time represented by Idaho Group basalts could be achieved by age dating of the ash and paleontological evaluation of the origin of conispiral gastropods and plant fragments present in the slightly cemented siltstone near the bottom of the hole. In the first scenario, the normal-reverse transition takes place ca. 4.2 Ma, while in the second scenario, the normal-reverse transition takes place ca. 3.4 Ma (Fig. 5).

Petrologic Evolution of Wendell Basalts

The major and trace element compositions, in conjunction with the geochemical depth-time relationships detailed above, imply the operation of several different processes throughout the volcanic history of the area intersected by the Wendell well and the central SRP. Some of the mechanisms that can operate within continental basalt systems include fractional crystallization (FC), bulk mixing (BM), and assimilation–FC (AFC).

Crystallization Models

Previously, workers suggested that the dominant process controlling the evolution of YSRP olivine tholeiite is low-pressure fractional crystallization of olivine and plagioclase (e.g., Leeman and Vitaliano, 1976; Leeman, 1982a, 1982b, 1982c; Geist et al., 2002b). We investigate this by using the FC–AFC–FCA–mixing Excel spreadsheet of Ersoy and Helvaci (2010). We model these processes by treating high-MgO compositions as parent magmas, two each from the Snake River Group and the Idaho Group. Lava flow 8b (parent magma 1: MgO = 9.55 wt%) and a hypothetical Snake River Group composition (parent magma 2) represent the parent magmas for Snake River Group basalts. Lava flows 51a (parent magma 3: MgO = 9.31 wt%) and 52b (parent magma 4: MgO = 9.16 wt%) represent the parent magmas for Idaho Group basalts. These lava flows are some of the most primitive lavas within their respective groups. Results are shown in Figure 6.

The models demonstrate that FC plays only a minor role in the formation of Wendell RASA basalts. In our model, the fractionating phases were olivine and plagioclase in a 40:60 ratio. Changing this ratio or even adding a small proportion of clinopyroxene as a fractionating phase does not change these results. In the Snake River Group, lava flows 5, 14, 16b, and 25 are on or close to the FC trend generated from parent magma 1 and represent 12%, 25%, and 40% FC, respectively (Fig. 6A). No lava flows can be generated by FC from the Snake River Group hypothetical parent (Fig. 6B). Within the Idaho Group, lava flows 40 and 32 are on or close to the FC trend generated from parent magma 3 and represent 20% and 35% FC, respectively (Fig. 6C). No samples are on the FC trend generated from parent magma 4 (Fig. 6D). Overall,

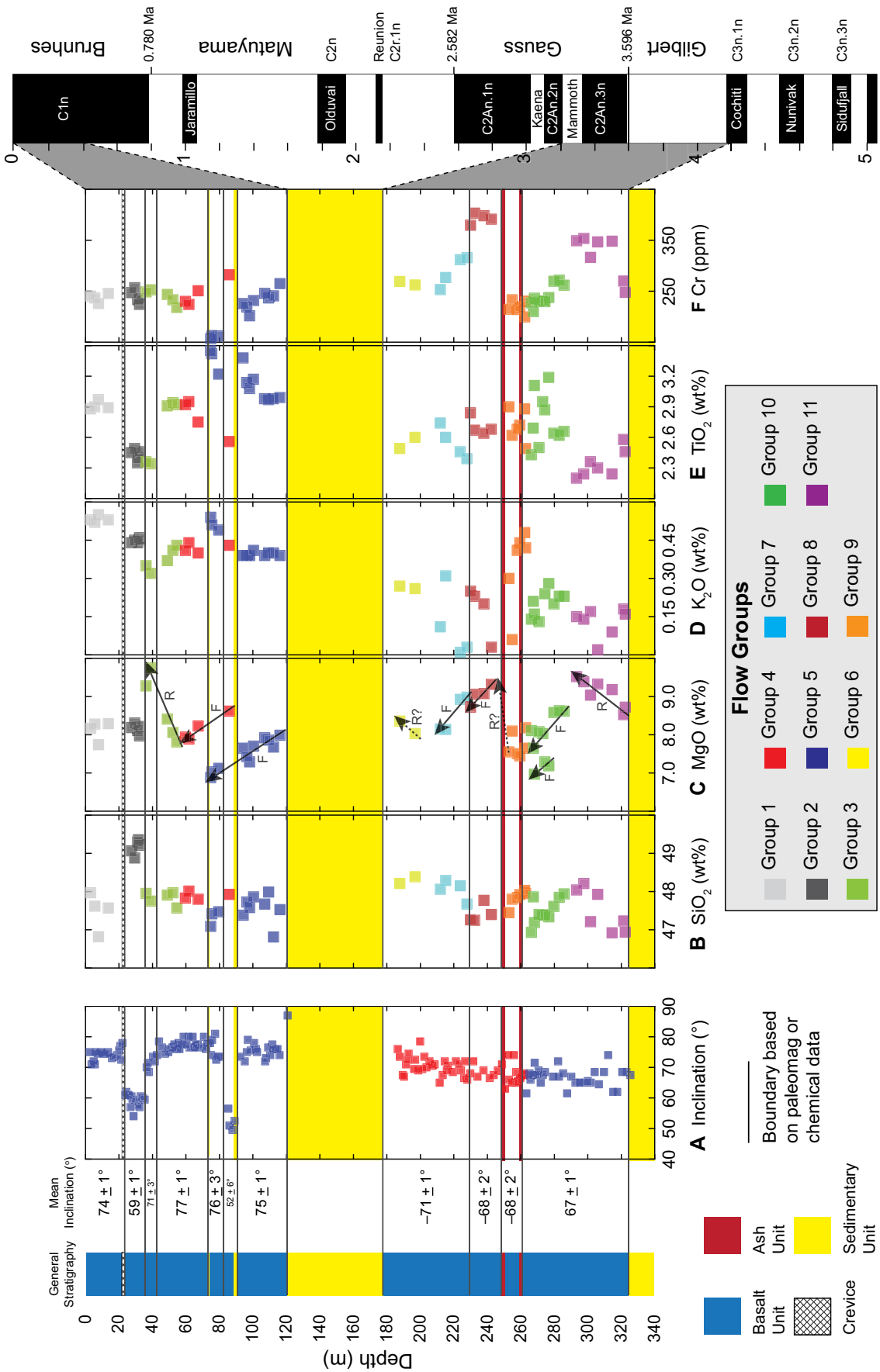

Figure 5. Comparison between a generalized stratigraphic column, mean paleomagnetic inclination, and the chemical composition of Wendell Regional Aquifer Systems Analysis (RASA) basalts, as a function of depth below surface (in meters). Polarity chrons are listed on right. (A) Paleomagnetic inclination data (same as Fig. 2B). The stratigraphic column has been further annotated with mean inclination values and 95% confidence levels for proposed boundaries between paleomagnetic and geochemical groups. (B–F) Wendell RASA major and trace element data versus depth (see text for discussion of chemical trends). We identify 11 flow groups, which are numbered from top to bottom: group 1 (3.1–13.6 mbs; 4 flows), group 2 (27.3–32.4 mbs; 5 flows), group 3 (36.2–54.6 mbs; 5 flows), group 4 (59.7–85.8 mbs; 4 flows), group 5 (74.8–116.1 mbs; 11 flows), group 6 (187.7–196.8 mbs; 2 flows), group 7 (211.9–227.9 mbs; 4 flows), group 8 (229.9–242.4 mbs; 4 flows), group 9 (252.9–262.9 mbs; 6 flows), group 10 (266.4–285.9 mbs; 10 flows), and group 11 (293.3–322.4 mbs; 7 flows). C is further annotated with arrows, displaying our interpretation of the fractionation (F) and recharge (R) cycles. Flow groups 4, 5, 7, 8, and 10 are interpreted as fractionation cycles, flow groups 3 and 11 are interpreted as recharge cycles, with possibly two additional recharge cycles (6, between 8 and 9), and flow groups 1 and 2 are neither. See text for discussion of chronostratigraphy of Snake River and Idaho Group basalts.

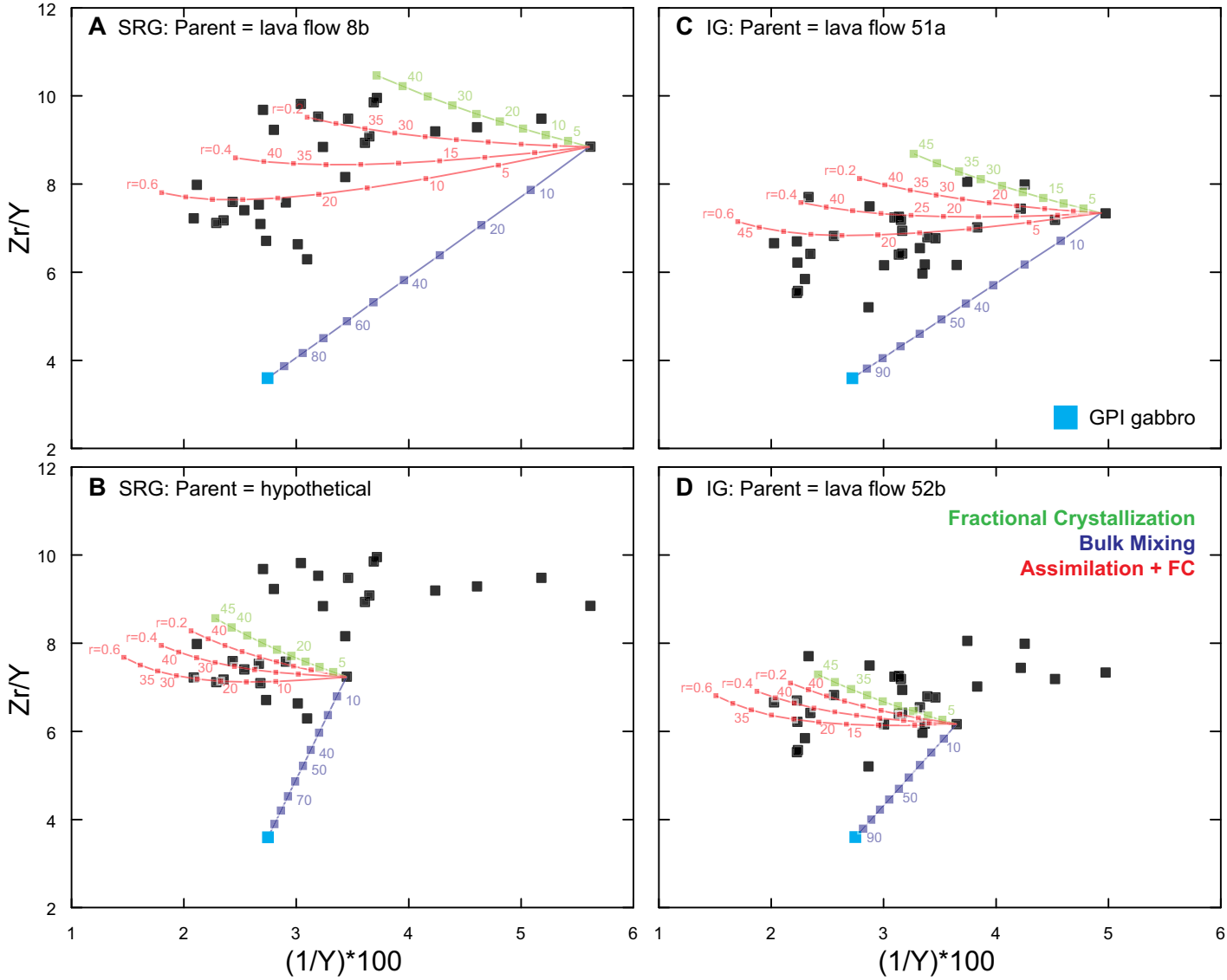

Figure 6. Crystallization models. (A, B) Snake River Group (SRG) basalts. (C, D) Idaho Group (IG) basalts. Fractional crystallization (FC) numbers are shown in percent crystallization, in increments of 5%; bulk mixing numbers are shown in percent assimilated, in increments of 10%. Assimilation–fractional crystallization numbers are shown in percent crystallization in increments of 5%; r ratios presented at end of corresponding line. GPI is Graveyard Point Intrusion.

fractional crystallization alone cannot account for the limited range in major element and trace element concentrations observed in Wendell RASA basalts.

In the scenario of two-component mass balance mixing, we mixed our parent magmas with an average composition for gabbroic rocks from the Graveyard Point Intrusion (White, 2007; gabbro includes granular gabbro, laminated gabbro, and poikilitic gabbro). The Graveyard Point Intrusion is located near the Oregon-Idaho boarder ~100 km west of Boise, Idaho. This pluton is a good model for shallow subvolcanic magma chambers in the YSRP because the chilled margins of the Graveyard Point Intrusion have a composition that is intermediate between high-alumina olivine tholeiites from the northwestern margin of the Basin and Range province and the more evolved olivine tholeiites typical of the younger (younger than 3 Ma) SRP basalts (White, 2007). It is clear that bulk mixing cannot replicate Wendell RASA basalt compositions because no Wendell RASA samples plot on any of the bulk mixing trends (Fig. 6). Therefore, bulk mixing is not a viable process within the central SRP.

Much of the chemical complexity shown by Wendell RASA basalts might be accounted for if crystallization were accompanied by assimilation (e.g., AFC). To further test AFC in the central plain, we assimilated the average Graveyard Point Intrusion gabbro composition used for the bulk mixing models, while fractionating our parent magma compositions. One important variable in these calculations is the r value, which represents the ratio of assimilated material to crystallized material (DePaolo, 1981). An r value of 0 represents fractional crystallization, while an r value of 1 represents bulk mixing. AFC agrees very well with the observed compositions from Wendell RASA, when r ranges from 0.2 to 0.6, modeled with 5% increments (Fig. 6). Most of the Zr/Y variation observed within the Snake River Group can be captured with 20%–60% assimilation of Graveyard Point

Intrusion gabbro, but requires as much as 45% crystallization (Figs. 6A, 6B). Similarly, Zr/Y variations observed within the Idaho Group can be captured with similar amounts of assimilation and crystallization (Figs. 6C, 6D). These AFC results are consistent with the hypothesis (Shervais et al., 2006a) for the partial assimilation of previously intruded mafic magmas by later YSRP basalts.

These models are not meant to reproduce the exact paths followed by Wendell RASA lavas, which is impossible without knowing the true assimilant and all parent magma compositions, but only to constrain the types of processes involved and their relative importance in controlling observed chemical trends.

Evidence of a Central SRP Mafic Sill Complex

Geophysical studies conducted in the eastern SRP (e.g., Sparlin et al., 1982; Peng and Humphreys, 1998; Humphreys et al., 2000) have imaged a relatively high velocity layer in the middle crust, with seismic velocities (~6.5 km/s) intermediate between mafic lower crust and the more felsic intermediate crust. This has been interpreted as a mid-crustal sill complex, measuring ~10 km thick by 90 km wide, with the top of the high-velocity layer at 15–25 km depth (Stachnik et al., 2008). This mafic sill is inferred to represent basaltic melts that were intruded into the crust, where magmas rose buoyantly and collected at their level of neutral buoyancy. Geochemical studies have confirmed this interpretation. Geist et al. (2002b) proposed that lavas sampled in the Test Area North drill core evolved by AFC of high-P_2O_5 ferrogabbro contained within a differentiated mafic intrusion emplaced at mid-crustal levels. Miller and Hughes (2009) suggested that the compositional variations expressed by surface vents and corehole USGS–132 resulted from mixing between chemically primitive and evolved compositions, where their end-member compositions are likely to be found in differentiated mafic sills in the crust.

There are several lines of evidence indicating that this sill complex extends into the central SRP. Geophysical evidence of a central SRP sill complex was advanced by Yuan et al. (2010), and they demonstrated, through shear velocities, that the mid-crustal layer starts at the northeast end of the eastern SRP beneath the Island Park caldera and extends to below the Picabo caldera (figs. 11A, 11B in Yuan et al., 2010). Beneath the Heise caldera field, the sill complex is between 18 and 32 km depth and is 14 km thick. At the southeast end of the eastern SRP, or underneath the central SRP, the top of this high-velocity mid-crustal layer deepens by ~5 km. Additional evidence is provided by cumulate gabbro xenoliths (olivine + clinopyroxene + plagioclase + Fe-Ti oxide) noted in some lava flows emanating from vents within the central SRP (e.g., Sid Butte: Matthews et al., 2006b).

CONCLUSIONS

This study provides one of the most complete examinations of the construction and evolution of the central SRP for the past 4 m.y. The Pliocene to Quaternary lavas sampled by the RASA well represent episodic eruptions from volcanoes similar to those observed on the surface today.

Using paleomagnetic data, in conjunction with geochemistry and borehole stratigraphy, we show that Wendell lavas were constructed on three different time scales: individual lava flows represent decadal to at most century time scales, geochemical groups (fractionation and recharge) represent multiple centuries for emplacement, and basalt groups (Snake River and Idaho) represent multimillennia time scales. These magnetic groupings are an important and independent confirmation of groupings based on chemistry. Although Wendell RASA basalts have major and trace element compositions similar to those of basalts from the eastern plain, we have shown that these lavas form a series of upward fractionation cycles and reversed cycles that represent fractionation of individual magma batches and progressive recharge of crustal magma chambers. We interpret that most of these cycles represent an eruption from one vent or plumbing system. However, the chemical stratigraphy supports the possibility, and likelihood, that two vents or plumbing systems were concurrently active. These interpretations are complicated by the fact that the manifestation of the geochemistry observed in the drill core occurred solely due to the different paths that the lava flows took over the future drill site. Eruptions, even a short distance away from the drill site, might not be sampled if the volcanic topography prevented flows from reaching the future drilling location. A reevaluation of the chemical stratigraphy at other SRP drill holes is warranted, given this possibility.

Fractionation of Wendell parent magmas was accompanied by assimilation of crustal material, but this crust could not have been ancient cratonic crust. Our models indicate that the dominant assimilant was previously intruded mafic rocks. Geophysical evidence points to a sill complex underlying the central SRP. The Graveyard Point Intrusion provides the best example of the mafic compositions necessary to assimilate with more primitive magmas to produce the observed trends. Fractional crystallization remains a possibility, but individual lava flows would require separate parent magmas. Further evidence of the influence of a central YSRP sill complex comes from the stratigraphic cyclic trends and the crystallization models, which resulted from mixing between chemically primitive and evolved compositions. The upward fractionation sequences are inferred to represent fractionation cycles identified in layered intrusions, whereas reversed intervals document the progressive influx of new magma batches. Each cycle may represent a single eruptive episode from a single volcano, or alternatively, individual volcanoes may include more than one fractionation-recharge cycle.

ACKNOWLEDGMENTS

We thank Keith Putirka and the X-ray fluorescence laboratory at California State University (Fresno) for helping with major element analysis; the inductively coupled plasma–mass spectrometry laboratory at Centenary College, Louisiana, for helping with trace element analysis; and Linda Davis and Mary Hodges at the Idaho National Laboratory Lithologic Core Storage Library for supplying all 340 m of Wendell Regional Aquifer Systems Analysis (RASA) core and for help with lithologic descriptions and pictures. Reviews by Eric Christiansen, Dennis Geist, Tyrone Rooney, Matt Brueseke, Bill Leeman, and an anonymous reviewer helped to improve this manuscript.

REFERENCES CITED

Armstrong, R.L., Leeman, W.P., and Malde, H.E., 1975, K-Ar dating, Quaternary and Neogene volcanic rocks of the Snake River Plain, Idaho: American Journal of Science, v. 275, p. 225–251, doi:10.2475/ajs.275.3.225.

Beranek, L.P., Link, P.K., and Fanning, C.M., 2006, Miocene to Holocene landscape evolution of the western Snake River Plain region, Idaho: Using the SHRIMP detrital zircon provenance record to track eastward migration of the Yellowstone hotspot: Geological Society of America Bulletin, v. 118, p. 1027–1050, doi: 10.1130/B25896.1.

Bonnichsen, B., and Godchaux, M., 2002, Late Miocene, Pliocene, and Pleistocene geology of southwestern Idaho with emphasis on basalts in the Bruneau-Jarbidge, Twin Falls, and western Snake River plain regions, *in* Bonnichsen, B., et al., eds., Tectonic and magmatic evolution of the Snake River Plain volcanic province: Idaho Geological Survey Bulletin 30, p. 233–312.

Champion, D.E., Lanphere, M.A., Anderson, S.R., and Kuntz, M.A., 2002, Accumulation and subsidence of the Pleistocene basaltic lava flows of the eastern Snake River plain, Idaho, *in* Link, P.K., and Mink, L.L., eds., Geology, hydrogeology, and environmental remediation: Idaho National Engineering and Environmental Laboratory, eastern Snake River Plain, Idaho: Geological Society of America Special Paper 353, p. 175–192, doi:10.1130/0-8137-2353-1.175.

Champion, D.E., Hodges, M.K.V., Davis, L.C., and Lanphere, M.A., 2011, Paleomagnetic correlation of surface and subsurface basaltic lava flows and flow groups in the southern part of the Idaho National Laboratory, Idaho, with paleomagnetic data tables for drill cores: U.S. Geological Survey Scientific Investigations Report 2011–5049, 34 p.

Cooke, M.F., Shervais, J.W., Kauffman, J.D., and Othberg, K.L., 2006a, Geologic map of the Dietrich Butte quadrangle, Lincoln County, Idaho: Idaho Geological Survey Digital Web Map DWM–63, scale 1:24,000.

Cooke, M.F., Shervais, J.W., Kauffman, J.D., and Othberg, K.L., 2006b, Geologic map of the Dietrich Quadrangle,

Lincoln County, Idaho: Idaho Geological Survey Digital Web Map DWM–66, scale 1:24,000.

Davis, L.C., Hannula, S.R., and Bowers, B., 1997, Procedures for use of, and drill cores and cuttings available for study at, the Lithologic Core Storage Library, Idaho National Engineering Laboratory, Idaho: U.S. Geological Survey Open-File Report 97-124, 31 p.

DePaolo, D.J., 1981, A neodymium and strontium isotopic study of the Mesozoic calc-alkaline granitic batholiths of the Sierra Nevada and Peninsula Ranges, California: Journal of Geophysical Research, v. 86, p. 10470–10488, doi:10.1029/JB086iB11p10470.

Ersoy, Y., and Helvaci, C., 2010, FC–AFC–FCA and mixing modeler: A Microsoft Excel spreadsheet program for modeling geochemical differentiation of magma by crystal fractionation, crustal assimilation and mixing: Computers & Geosciences, v. 36, p. 383–390, doi:10.1016/j.cageo.2009.06.007.

Geist, D.J., Teasdale, R., Sims, E., and Hughes, S., 2002a, Subsurface volcanology at Test Area North and controls on groundwater flow, *in* Link, P.K., and Mink, L.L., eds., Geology, hydrogeology, and environmental remediation: Idaho National Engineering and Environmental Laboratory, eastern Snake River Plain, Idaho: Geological Society of America Special Paper 353, p. 45–59, doi:10.1130/0-8137-2353-1.45.

Geist, D.J., Sims, E.N., Hughes, S.S., and McCurry, M., 2002b, Open-system evolution of a single episode of Snake River Plain magmatism, *in* Link, P.K., and Mink, L.L., eds., Geology, hydrogeology, and environmental remediation: Idaho National Engineering and Environmental Laboratory, eastern Snake River Plain, Idaho: Geological Society of America Special Paper 353, p. 193–204, doi:10.1130/0-8137-2353-1.193.

Gradstein, F.M., Ogg, J.G., and Smith, A.G., 2005, A geologic time scale 2004: Cambridge, UK, Cambridge University Press, 589 p.

Greeley, R., 1982, The Snake River Plain, Idaho: Representative of a new category of volcanism: Journal of Geophysical Research, v. 87, no. B4, p. 2705–2712, doi:10.1029/JB087iB04p02705.

Hanan, B.B., Shervais, J.W., and Vetter, S.K., 2008, Yellowstone plume–continental lithosphere interaction beneath the Snake River Plain: Geology, v. 36, p. 51–54, doi:10.1130/G23935A.1.

Hart, W.K., and Brueseke, M.E., 1999, Analysis and dating of volcanic horizons from Hagerman Fossil Beds National Monument and a revised interpretation of Eastern Glenns Ferry Formation chronostratigraphy. A report of work accomplished and scientific results: Hagerman, Idaho, Hagerman Fossil Beds National Monument, 37 p.

Hodges, M.K.V., Link, P.K., and Fanning, C.M., 2009, The Pliocene Lost River found to west: Detrital zircon evidence of drainage disruption along a subsiding hotspot track: Journal of Volcanology and Geothermal Research, v. 188, p. 237–249, doi:10.1016/j.jvolgeores.2009.08.019.

Honjo, N., Bonnichsen, B., Leeman, W.P., and Stormer, J.C., 1992, Mineralogy and geothermometry of high-temperature rhyolites from the central and western Snake River Plain: Bulletin of Volcanology, v. 54, p. 220–237, doi:10.1007/BF00278390.

Hughes, S.S., McCurry, M., and Geist, D.J., 2002, Geochemical correlations and implications for the magmatic evolution of basalt flow groups at the Idaho National Engineering and Environmental Laboratory, *in* Link, P.K., and Mink, L.L., eds., Geology, hydrogeology, and environmental remediation: Idaho National Engineering and Environmental Laboratory, eastern Snake River Plain, Idaho: Geological Society of America Special Paper 353, p. 151–173, doi:10.1130/0-8137-2353-1.151.

Humphreys, E.D., Dueker, K.G., Schutt, D.L., and Smith, R.B., 2000, Beneath Yellowstone: Evaluating plume and nonplume models using teleseismic images of the upper mantle: GSA Today, v. 10, p. 1–6.

Jenner, G.A., Longerich, H.P., Jackson, S.E., and Fryer, B.J., 1990, ICP–MS—A powerful tool for high-precision trace-element analysis in Earth Science: Evidence from analysis of selected U.S.G.S. reference samples: Chemical Geology, v. 83, p. 133–148, doi:10.1016/0009-2541(90)90145-W.

Kauffman, J.D., and Othberg, K.L., 2004, Geologic map of the Wendell quadrangle, Gooding County, Idaho: Idaho Geological Survey Digital Web Map DWM–23, scale 1:24,000.

Kauffman, J.D., Othberg, K.L., Shervais, J.W., and Matthews, S.H., 2005, Geologic map of the Shoshone quadrangle, Lincoln County, Idaho: Idaho Geological Survey Digital Web Map DWM–44, scale: 1:24,000.

Kauffman, J.D., Othberg, K.L., Gillerman, V.S., and Garwood, D.L., 2011, Geologic map of the Twin Falls 30 × 60 minute quadrangle, Idaho: Idaho Geological Survey Digital Web Map DWM–43–M, scale 1:100,000.

Kuntz, M.A., Champion, D.E., Spiker, E.C., Lefebvre, R.H., and McBroome, L.A., 1982, The Great Rift and the evolution of the Craters of the Moon lava field, Idaho, *in* Bonnichsen, B., and Breckenridge, R.M., eds., Cenozoic Geology of Idaho: Idaho Bureau of Mines and Geology Bulletin 26, p. 423–437.

Kuntz, M.A., Covington, H.R., and Schorr, L.J., 1992, An overview of basaltic volcanism of the eastern Snake River Plain, Idaho, *in* Link, P.K., et al., eds., Regional geology of eastern Idaho and western Wyoming: Geological Society of America Memoir 179, p. 227–267, doi:10.1130/MEM179-p227.

Le Bas, M.J., Le Maitre, R.W., Streckeisen, A.L., and Zanettin, B., 1986, A chemical classification of volcanic rocks based on the total alkali–silica diagram: Journal of Petrology, v. 27, p. 745–750, doi:10.1093/petrology/27.3.745.

Leeman, W.P., 1982a, Olivine tholeiitic basalts of the Snake River Plain, Idaho, *in* Bonnichsen B., and Breckenridge, R.M., eds., Cenozoic geology of Idaho: Idaho Bureau of Mines and Geology Bulletin, v. 26, p. 181–191.

Leeman, W.P., 1982b, Development of the Snake River Plain–Yellowstone Plateau Province, Idaho and Wyoming: An overview and petrologic model, *in* Bonnichsen, B., and Breckenridge, R.M., eds., Cenozoic geology of Idaho: Idaho Bureau of Mines and Geology Bulletin 26, p. 155–177.

Leeman, W.P., 1982c, Evolved and hybrid lavas from the Snake River Plain, Idaho, *in* Bonnichsen, B., and Breckenridge, R.M., eds., Cenozoic geology of Idaho: Idaho Bureau of Mines and Geology Bulletin 26, p. 193–202.

Leeman, W.P., and Vitaliano, C.J., 1976, Petrology of McKinney Basalt, Snake River Plain, Idaho: Geological Society of America Bulletin, v. 87, p. 1777–1792, doi:10.1130/0016-7606(1976)87<1777:POMBSR>2.0.CO;2.

Le Maitre, R.W., 1976, The chemical variability of some common igneous rocks: Journal of Petrology, v. 17, p. 589–598, doi:10.1093/petrology/17.4.589.

Link, P.K., and Mink, L.L, eds., 2002, Geology, hydrogeology, and environmental remediation: Idaho National Engineering and Environmental Laboratory, eastern Snake River Plain, Idaho: Geological Society of America Special Paper 353, 296 p., doi:10.1130/0-8137-2353.

Link, P.K., McDonald, H.G., Fanning, C.M., and Godfrey, A.E., 2002, Detrital zircon evidence for Pleistocene drainage reversal at Hagerman Fossil Beds National Monument, central Snake River Plain, Idaho, *in* Bonnichsen, B., et al., eds., Tectonic and magmatic evolution of the Snake River Plain Volcanic Province: Idaho Geological Survey Bulletin 30, p. 105–119.

Matthews, S.H., Shervais, J.W., Kauffman, J.D., and Othberg, K.L., 2006a, Geologic map of the Shoshone SE quadrangle, Jerome and Lincoln Counties, Idaho: Idaho Geological Survey Digital Web Map DWM–62, scale 1:24,000.

Matthews, S.H., Shervais, J.W., Kauffman, J.D., and Othberg, K.L., 2006b, Geologic map of the Star Lake quadrangle, Jerome and Lincoln Counties, Idaho: Idaho Geological Survey Digital Web Map DWM–67, scale 1:24,000.

McDonough, W.F., and Sun, S.-s., 1995, The composition of the Earth: Chemical Geology, v. 120, p. 223–253, doi:10.1016/0009-2541(94)00140-4.

McFadden, P.L., and Reid, A.B., 1982, Analysis of paleomagnetic inclination data: Royal Astronomical Society Geophysical Journal, v. 69, p. 307–319, doi:10.1111/j.1365-246X.1982.tb04950.x.

Miller, M.L., and Hughes, S.S., 2009, Mixing primitive and evolved olivine tholeiite magmas in the Eastern Snake River Plain, Idaho: Journal of Volcanology and Geothermal Research, v. 188, p. 153–161, doi:10.1016/j.jvolgeores.2009.06.004.

Neal, C.R., 2001, The interior of the Moon: The presence of garnet in the primitive, deep lunar mantle: Journal of Geophysical Research, v. 106, p. 27865–27885, doi:10.1029/2000JE001386.

Oakley, W.L., III, and Link, P.K., 2006, Geologic map of the Davis Mountain quadrangle, Gooding and Camas Counties, Idaho: Idaho Geologic Survey Technical Report T-06–6, scale 1:24,000.

Peng, X., and Humphreys, E.D., 1998, Crustal velocity structure across the eastern Snake River Plain and the Yellowstone swell: Journal of Geophysical Research, v. 103, no. B4, p. 7171–7186, doi:10.1029/97JB03615.

Perkins, M.E., Nash, W.P., Brown, F.H., and Fleck, R.J., 1995, Fallout tuffs of Trapper Creek Idaho—A record of Miocene explosive volcanism in the Snake River Plain volcanic province: Geological Society of America Bulletin, v. 107, p. 1484–1506, doi:10.1130/0016-7606(1995)107<1484:FTOTCI>2.3.CO;2.

Pierce, K.L., and Morgan, L.A., 1992, The track of the Yellowstone hotspot: Volcanism, faulting, and uplift, *in* Link, P.K., et al., eds., Regional geology of eastern Idaho and western Wyoming: Geological Society of America Memoir 179, p. 1–54, doi:10.1130/MEM179-p1.

Pierce, K.L., Morgan, L.A., and Saltus, R.W., 2002, Yellowstone plume head: Postulated tectonic relations to the Vancouver slab, continental boundaries, and climate, *in* Bonnichsen, B., et al., eds., Tectonic and magmatic evolution of the Snake River Plain Volcanic Province: Idaho Geological Survey Bulletin 30, p. 5–33.

Potter, K.E., Shervais, J.W., and Sant, C.J., 2011, Project Hotspot: Insight into the subsurface stratigraphy and geothermal potential of the Snake River Plain: Geothermal Resources Council Transactions, v. 35, p. 967–971.

Ruez, D.R., 2009, Framework for stratigraphic analysis of Pliocene fossiliferous deposits at Hagerman Fossil Beds National Monument, Idaho: Rocky Mountain Geology, v. 44, no. 1, p. 33–70, doi:10.2113/gsrocky.44.1.33.

Sadler, J.L., and Link, P.K., 1996, The Tuana Gravel: Early Pleistocene response to longitudinal drainage of a late-stage rift basin, western Snake River Plain, Idaho: Northwest Geology, v. 26, p. 46–62.

Shervais, J.W., Kauffman, J.D., Gillerman, V.S., Othberg, K.L., Vetter, S.K., Hobson, V.R., Zarnetske, M., Cooke, M.F., Matthews, S.H., and Hanan, B.B., 2005, Basaltic volcanism of the central and western Snake River Plain: A guide to field relations between Twin Falls and Mountain Home, Idaho, *in* Pederson, J., and Dehler, C.M., eds., Interior western United States: Geological Society of America Field Guide 6, p. 27–52, doi:10.1130/2005.fld006(02).

Shervais, J.W., Vetter, S.K., and Hanan, B.B., 2006a, A layered mafic sill complex beneath the eastern Snake River Plain: Evidence from cyclic geochemical variations in basalt: Geology, v. 34, p. 365–368, doi:10.1130/G22226.1.

Shervais, J.W., Cooke, M.F., Kauffman, J.D., and Othberg, K.L., 2006b, Geologic map of the Owinza quadrangle, Lincoln County, Idaho: Idaho Geological Survey Digital Web Map DWM–64, scale 1:24,000.

Shervais, J.W., Cooke, M.F., Kauffman, J.D., and Othberg, K.L., 2006c, Geologic map of the Owinza Butte quadrangle, Jerome and Lincoln Counties, Idaho: Idaho Geological Survey Digital Web Map DWM–65, scale 1:24,000.

Shervais, J.W., Evans, J.P., Christiansen, E.H., Schmitt, D.R., Kessler, J.A., Potter, K.E., Jean, M.M., Sant, C.J., and Freeman, T.G., 2011, Project Hotspot—The Snake River Scientific Drilling Project: Geothermal Resources Council Transactions, v. 35, p. 995–1003.

Shervais, J.W., and 16 others, 2012, Hotspot: The Snake River Geothermal Drilling Project—Initial report: Geothermal Resources Council Transactions, v. 36, p. 767–772.

Smith, R.B., and Braile, L.W., 1993, Topographic signature, space-time evolution, and physical properties of

the Yellowstone–Snake River Plain volcanic system: The Yellowstone hotspot, *in* Snoke, A.W., et al., eds., Geology of Wyoming: Geological Survey of Wyoming Memoir 5, p. 694–754.

Smith, R.B., and Braile, L.W., 1994, The Yellowstone hotspot: Journal of Volcanology and Geothermal Research, v. 61, p. 121–187, doi:10.1016/0377-0273(94)90002-7.

Sparlin, M.A., Braile, L.W., and Smith, R.B., 1982, Crustal structure of the eastern Snake River Plain determined from ray trace modeling of seismic refraction data: Journal of Geophysical Research, v. 87, p. 2619–2633, doi:10.1029/JB087iB04p02619.

Stachnik, J.C., Dueker, K., Schutt, D.L., and Yuan, H., 2008, Imaging Yellowstone plume–lithosphere interactions from inversion of ballistic and diffusive Rayleigh wave dispersion and crustal thickness data: Geochemistry Geophysics Geosystems, v. 9, no. 6, doi:10.1029/2008GC001992.

Tauxe, L., Luskin, C., Selkin, P., Gans, P., and Calvert, A., 2004, Paleomagnetic results from the Snake River Plain: Contribution to the time-averaged field global database: Geochemistry Geophysics Geosystems, v. 5, no. 8, doi:10.1029/2003GC000661.

White, C.M., 2007, The Graveyard Point Intrusion: An example of extreme differentiation of Snake River Plain Basalt in a shallow crustal pluton: Journal of Petrology, v. 48, p. 303–325, doi:10.1093/petrology/egl062.

Whitehead, R.L., and Lindholm, G.F., 1985, Results of geohydrologic test drilling in the Eastern Snake River Plain, Gooding County, Idaho: U.S. Geological Survey Water-Resources Investigations Report 84-4294, 30 p.

Yuan, H., Dueker, K., and Stachnik, J., 2010, Crustal structure and thickness along the Yellowstone hot spot track: Evidence for lower crustal outflow from beneath the eastern Snake River Plain: Geochemistry Geophysics Geosystems, v. 11, no. 3, 14 p., doi:10.1029/2009GC002787.